Cooperative decentralized navigation algorithms based on bearing measurements for arbitrary measurement topologies

Pedro Mendes, Pedro Batista, Paulo Oliveira, and Carlos Silvestre

Ocean Engineering, vol. 270, 113564, February 2023

https://doi.org/10.1016/j.oceaneng.2022.113564

Cite as: Pedro Mendes, Pedro Batista, Paulo Oliveira, and Carlos Silvestre, "Cooperative decentralized navigation algorithms based on bearing measurements for arbitrary measurement topologies," Ocean Engineering, vol. 270, 113564, February 2023.

Ocean Engineering 270 (2023) 113564

Contents lists available at ScienceDirect

Ocean Engineering

journal homepage: www.elsevier.com/locate/oceaneng

Cooperative decentralized navigation algorithms based on bearing measurements for arbitrary measurement topologies

Pedro Mendes [a,*], Pedro Batista [a], Paulo Oliveira [a,b], Carlos Silvestre [a,c]

[a] Institute for Systems and Robotics, Instituto Superior Técnico, Universidade de Lisboa, Lisboa 1049-001, Portugal
[b] LAETA—Associated Laboratory for Energy, Transports and Aeronautics, IDMEC—Institute of Mechanical Engineering, Instituto Superior Técnico, Universidade de Lisboa, Lisboa 1049-001, Portugal
[c] Faculty of Science and Technology, University of Macau, Taipa, Macao

ARTICLE INFO

Keywords:
Decentralized navigation
Kalman filtering
Position and fluid-velocity estimation

ABSTRACT

This work presents and compares several cooperative navigation solutions for formations of autonomous underwater vehicles, equipped with depth sensors and capable of taking bearing measurements to their neighbors under a certain measurement topology. Two approaches based on the extended Kalman filter are described, one centralized and the other decentralized, which has the advantage of requiring much less communication and computational complexity with minimal degradation of the produced estimates. Additionally, four other Kalman filter implementations, based on systems with linear dynamics using artificial measurements, are also described, one centralized and the remaining ones decentralized. The performance of these algorithms, under both acyclical and cyclical measurement topologies, is compared using Monte Carlo simulations, whereby both the mean error and root-mean-squared-error (RMSE) of the computed navigation estimates are presented.

1. Introduction

Advances in technology in the past years have brought increased interest towards the development of autonomous vehicles. Not only do these allow for missions which come at minimal risk for humans, but they also allow for use of cheaper and smaller vehicles, since they do not need to be manned. This makes autonomous vehicles a very captivating technology for activities such as surveillance, scientific exploration, resource gathering, and rescue missions, among others.

An essential part of a system of autonomous vehicles is the localization aspect, which is more challenging in underwater applications due to the lack of reliable access to satellite navigation systems. Because of this, underwater localization must be performed via relative measurements and information exchange between agents. Due to the underwater attenuation of the electromagnetic spectrum used for conventional communication, centralized approaches might become impractical due to bandwidth or range restrictions. In recent years, there has been an increasing interest in performing missions with a high number of agents, which for most applications need to be localized. Furthermore, the specific mission might require the agents to maintain a specific formation, for which correct localization becomes even more essential in order for the control problem to be tractable. This increase in number of agents makes it so centralized estimation algorithms become impractical. Thus, there is a need for decentralized navigation algorithms, which scale better with the number of agents and are possibly more robust.

In this work, the problem of decentralized state estimation for an underwater vehicle formation is considered, whereby the agents attempt to localize themselves and estimate their local fluid velocity through measurements and information exchange with their neighbors. In previous work by the authors Mendes and Batista (2021), a comparison of the two extended Kalman filter based algorithms discussed in this work was made, and the effect of the measurement topology on their performance was also studied. In the referenced work, it was concluded that, while the centralized version of the estimator presented slightly better position estimation capabilities, it requires a much larger amount of communication between agents and suffers from a large additional computational complexity, making the decentralized algorithm a better fit in most cases. However, it was assumed that the agents have access to noiseless attitude measurements, which is never the case. This work expands upon this previous study by introducing attitude measurement noise, as well as other approaches, which rely on the definition of artificial measurements and thus can present global error

* Corresponding author.
E-mail addresses: pedro.a.mendes@tecnico.ulisboa.pt (P. Mendes), pbatista@isr.tecnico.ulisboa.pt (P. Batista), paulo.j.oliveira@tecnico.ulisboa.pt (P. Oliveira), csilvestre@umac.mo (C. Silvestre).

https://doi.org/10.1016/j.oceaneng.2022.113564
Received 22 January 2022; Received in revised form 11 December 2022; Accepted 26 December 2022
Available online 10 January 2023

convergence under certain conditions. Moreover, extensive simulation results are presented here for all approaches, considering always noisy measurements With this study, it is our goal to provide insight on the strengths and weaknesses of each approach, so that this information is also available when choosing a navigation algorithm to perform a certain mission.

1.1. Related work

Much work has been done on the subject of decentralized navigation. Some approaches, including the ones presented in this work, have their basis on the widely used Kalman filter, which remains a powerful tool when it comes to state estimation in the presence of Gaussian white noise.

In Fallon et al. (2010), the authors attempt to replicate the centralized Kalman filter by using a communication scheme to distribute all dead-reckoning and measurement information between agents, such that they can all manage a centralized Kalman filter with all the information. This approach does not take advantage of the benefits of decentralization, such as scalability, and requires too much communication between agents, which is not desirable. Other works, such as Bahr et al. (2009), also attempt to reproduce the centralized filter through bookkeeping strategies. In Carrillo-Arce et al. (2013), the authors present a decentralized solution based on the covariance intersection algorithm to build a consistent Kalman filter estimator, guaranteeing that its estimates do not become overconfident, which is important in order to prevent divergence of solutions based on the extended Kalman filter (Kia et al., 2016). More recently, Luft et al. (2018) presented a decentralized algorithm which approximates the centralized Kalman filter while requiring very limited communication between neighbors and showing good scalability. This algorithm is applied in this work, considering bearing and depth measurements in an extended Kalman filter version of the algorithm, as well as modified version, which uses the definition of an artificial output. The considered system output is based on the work Santos et al. (2021), whereby independent observers are designed using a bearing-based artificial output, which guarantees global asymptotic stability in acyclical formations. Another approached based on the Kalman filter for linear time-invariant systems is presented in Viegas et al. (2018), whereby the authors present a method for computing gain matrices for each agent. This approach is also used in this work by applying the method for computing the gain matrices to artificially constructed position difference measurements.

The topic of decentralized navigation of autonomous vehicle formations is closely related to that of localizing a mobile sensor network using only local information exchange and measurements at each node. As an example, Safavi et al. (2018) presents an algorithm to globally localize a sensor network using range measurements. This is achieved by transforming such a set of range measurements into barycentric coordinates, which then allows for writing an update rule with globally convergent error dynamics.

The remaining of this paper is organized as follows. In Section 2, the navigation problem is formally described, and in Section 3, two approaches based on the extended Kalman filter are presented, one is a centralized extended Kalman filter implementation, and the other is a decentralized technique, presented in Luft et al. (2018). In Section 4, approaches based on rewriting the measurement model considering artificial outputs are described, whereby linear Kalman filters are implemented on these artificial systems, as done in Santos et al. (2021). Finally, in Section 5, the approaches considered in this work are evaluated and their performances compared, making use of Monte Carlo results obtained via simulation.

1.2. Notation

In this section, the notation adopted throughout this work is defined. Vectors and matrices are represented in bold and their scalar entries are superscripted, such that $\mathbf{v} = (\mathbf{v}^i) \in \mathbb{R}^n$ and $\mathbf{A} = (\mathbf{A}^{ij}) \in \mathbb{R}^{m\times n}$. The identity and zero square matrices of size n are represented as $\mathbf{I}_n$ and $\mathbf{0}_n$, respectively. If the zero matrix is not square, then it is represented as $\mathbf{0}_{m\times n} \in \mathbb{R}^{m\times n}$. The transpose operator is represented by $(\cdot)^T$ and $\mathrm{diag}(\cdot)$ builds a diagonal matrix from the arguments. Additionally, the Kronecker product is denoted by the symbol $\otimes$, such that, for $\mathbf{A} \in \mathbb{R}^{m\times n}$, $\mathbf{B} \in \mathbb{R}^{p\times q}$, one has

$$A \otimes B := \begin{bmatrix} \mathbf{A}^{11}\mathbf{B} & \cdots & \mathbf{A}^{1n}\mathbf{B} \\ \vdots & \ddots & \vdots \\ \mathbf{A}^{m1}\mathbf{B} & \cdots & \mathbf{A}^{mn}\mathbf{B} \end{bmatrix} \in \mathbb{R}^{pm\times qn}.$$

If $\mathcal{S}$ denotes a set, $|\mathcal{S}|$ represents its cardinality, i.e., the number of elements in $\mathcal{S}$.

2. Problem statement

Consider a set of AUVs, numbered from 1 to N, operating in a 3D environment such that the movement of each AUV in the inertial frame, $\{I\}$, is described by

$$\begin{cases} \dot{\mathbf{p}}_i(t) = \mathbf{R}_i(t)\mathbf{v}_{r_i}(t) + \mathbf{v}_{f_i}(t) \\ \dot{\mathbf{v}}_{f_i}(t) = \mathbf{0}_3 \end{cases},$$

for $i \in \{1,\ldots,N\}$, where $\mathbf{p}_i(t) = \begin{bmatrix} \mathbf{p}_i^x(t) & \mathbf{p}_i^y(t) & \mathbf{p}_i^z(t) \end{bmatrix}^T \in \mathbb{R}^3$ represents the position of the ith AUV, $\mathbf{R}_i \in SO(3)$ is the rotation matrix that describes the attitude of the ith AUV, transforming coordinates in its body frame to coordinates in the inertial frame, $\mathbf{v}_{r_i}(t)$ is the velocity of the ith AUV with respect to the fluid it is operating in, represented in the AUV's body frame, and $\mathbf{v}_{f_i}(t)$ is the local velocity of the fluid where the ith AUV is operating, expressed in the inertial frame.

Remark 1. Note that, in practical terms, $\mathbf{v}_{f_i}$ is a function of both time and the position, $\mathbf{p}_i$, of the agent. Indeed: (i) the velocity of the fluid at a fixed position may change over time; and (ii) the velocity of the fluid may not be uniform with respect to the inertial position. Hence, as the ith AUV moves over time, the local velocity of the fluid where it operates may change over time, either due to the change in position of the ith AUV, time lapse, or both. However, in nominal terms, and for modeling purposes for each agent, it is assumed to be constant, which is a reasonable model approximation considering that, in most cases, the velocity of the fluid is slowly time-varying. In practice, by appropriate tuning of the parameters of the filtering solution, it is possible to estimate slowly time-varying quantities, as many filters assume the presence of random additive process noise. This is a standard approach to model such quantity.

Since solutions are usually implemented on a digital computer, the continuous-time kinematics must be discretized, resulting in

$$\begin{cases} \mathbf{p}_i(t_{k+1}) = \mathbf{p}_i(t_k) + T\mathbf{v}_{f_i}(t_k) + \mathbf{u}_i[k] \\ \mathbf{v}_{f_i}(t_{k+1}) = \mathbf{v}_{f_i}(t_k) \end{cases}, \tag{1}$$

where

$$\mathbf{u}_i[k] = \int_{t_k}^{t_{k+1}} \mathbf{R}_i(t)\mathbf{v}_{r_i}(t)dt \tag{2}$$

and T is the sampling time. In state-space form, letting the state of the ith agent be defined as

$$\mathbf{x}_i[k] := \begin{bmatrix} \mathbf{p}_i(t_k) \\ \mathbf{v}_{f_i}(t_k) \end{bmatrix} \in \mathbb{R}^6, \tag{3}$$

and following (1), the motion model of an agent is given by

$$\mathbf{x}_i[k+1] = \mathbf{A}\mathbf{x}_i[k] + \mathbf{B}\mathbf{u}_i[k],$$

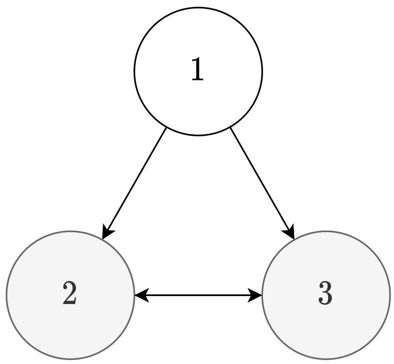

Fig. 1. Example measurement graph.

where

$$\mathbf{A} := \begin{bmatrix} \mathbf{I}_3 & T\mathbf{I}_3 \\ \mathbf{0}_3 & \mathbf{I}_3 \end{bmatrix} \tag{4}$$

and

$$\mathbf{B} := \begin{bmatrix} \mathbf{I}_3 \\ \mathbf{0}_3 \end{bmatrix}. \tag{5}$$

The AUVs are equipped with sensors that enable them to make measurements about themselves, such as depth and attitude measurements; and about their neighbors, such as bearing measurements. In addition to this, they are also capable of some degree of communication between themselves, enabling them to share quantities, such as position estimates, with their neighbors.

At this point, it is assumed that if the jth AUV is capable of taking measurements about the ith agent, then there is a bidirectional communication link between the two. The formation's measurement configuration can then be represented with a single directed graph $\mathcal{G} := (\mathcal{V}, \mathcal{E})$, where $\mathcal{V}$ is the set of AUVs and $\mathcal{E}$ is the set of directed edges, representing measurement information flow. The jth AUV takes measurements about the ith AUV if there is a directed edge leaving node i and entering node j, i.e., if there is an edge $e_{ij} = (i, j)$. The neighbor set of the ith AUV is then defined as the set of AUVs that it takes measurements about, i.e., $\mathcal{N}_i = \{j : (j, i) \in \mathcal{E}\}$. It is also assumed that $\mathcal{V}$ can be further separated into two disjoint subsets, $\mathcal{V}_\mathcal{L}$ and $\mathcal{V}_\mathcal{F}$, such that $\mathcal{V}_\mathcal{L} \cup \mathcal{V}_\mathcal{F} = \mathcal{V}$. The set $\mathcal{V}_\mathcal{L}$ contains the so-called *leader* AUVs, which are assumed to able to estimate their position with some accuracy by themselves, and the set $\mathcal{V}_\mathcal{F}$ contains the *follower* AUVs, that must estimate their state based on measurements about their neighbors and communication with them.

Example 1. Consider the measurement graph, $\mathcal{G}$, presented in Fig. 1. In this example, the leader set is $\mathcal{V}_\mathcal{L} = \{1\}$ and the follower set is $\mathcal{V}_\mathcal{F} = \{2, 3\}$, which is graphically represented with grayed out nodes. As per the previous definitions, the 2nd AUV takes measurements about and receives information from the 1st and 3rd agents. Likewise for the 3rd AUV, which takes measurements about agents 1 and 2, one has $\mathcal{N}_3 = \{1, 2\}$. The neighbor sets of the AUVs 1 and 2 are $\mathcal{N}_1 = \emptyset$ and $\mathcal{N}_2 = \{1, 3\}$, respectively.

Consider now that the AUVs in $\mathcal{V}_\mathcal{F}$ are equipped with pressure gauges and attitude and heading reference systems, so that they can determine their own depth and orientation, as well some sensor that allows them to measure bearings to neighboring AUVs. As an example, an ultra-short baseline acoustic positioning system readily gives bearing measurements (Reis et al., 2016). Then, according to the measurement graph, at time t_k, in addition to its noisy attitude measurement, given by its rotation matrix, AUV 3 has access to the following information

$$\begin{cases} z_3(t_k) = \mathbf{p}_3^z(t_k) + e_1(t_k) \\ \theta_{31}(t_k) = {}^{\mathcal{B}}\theta(\mathbf{p}_3(t_k), \mathbf{p}_1(t_k)) + e_2(t_k) \\ \phi_{31}(t_k) = {}^{\mathcal{B}}\phi(\mathbf{p}_3(t_k), \mathbf{p}_1(t_k)) + e_3(t_k) \\ \theta_{32}(t_k) = {}^{\mathcal{B}}\theta(\mathbf{p}_3(t_k), \mathbf{p}_2(t_k)) + e_4(t_k) \\ \phi_{32}(t_k) = {}^{\mathcal{B}}\phi(\mathbf{p}_3(t_k), \mathbf{p}_2(t_k)) + e_5(t_k) \\ \hat{\mathbf{p}}_1(t_k) = \mathbf{p}_1(t_k) + \mathbf{e}_6(t_k) \\ \hat{\mathbf{p}}_2(t_k) = \mathbf{p}_2(t_k) + \mathbf{e}_7(t_k) \end{cases},$$

where $\mathbf{p}_3$ represents the position of AUV 3, $\hat{\mathbf{p}}_j$ is a position estimate of AUV $j \in \{1, 2\}$ that is communicated to AUV 3, ${}^{\mathcal{B}}\theta(\mathbf{p}_i, \mathbf{p}_j)$ and ${}^{\mathcal{B}}\phi(\mathbf{p}_i, \mathbf{p}_j)$ are functions that return the noiseless bearing angles, measured by an agent with index i about another agent with index j, represented in agent i's body frame. The quantities e_1, e_2, e_3, e_4, e_5, $\mathbf{e}_6$, and $\mathbf{e}_7$ are unknown errors terms, due to, for instance, measurement noise or estimation errors.

Considering the measured bearing angles, θ_{ij} and ϕ_{ij}, these can be used to construct the direction vector from agent i to agent j represented in the inertial frame, $\mathbf{d}_{ij}$, through

$$\begin{aligned} \mathbf{d}_{ij}(t_k) &= \mathbf{R}_i(t_k) \begin{bmatrix} \cos\theta_{ij}(t_k)\cos\phi_{ij}(t_k) \\ \cos\theta_{ij}(t_k)\sin\phi_{ij}(t_k) \\ \sin\theta_{ij}(t_k) \end{bmatrix} \\ &= \frac{\mathbf{p}_j(t_k) - \mathbf{p}_i(t_k)}{\|\mathbf{p}_j(t_k) - \mathbf{p}_i(t_k)\|}, \end{aligned} \tag{6}$$

where the last equality holds given noiseless attitude and bearing measurements. Note that the rotation matrix built from the noisy attitude angles, $\mathbf{R}_i(t_k)$, is used both in (6) and (2). While this is not approached in this work, there could be a correlation between the system model and the measurement model errors in the presented approaches, which could end up pushing the steady-state estimates away from the true state of the system. In practice, simulation results show that the proposed solutions are not affected, at least significantly, by any correlation effects between noises.

The decentralized navigation problem addressed in this paper is to estimate the position $\mathbf{p}_i(t)$ of each AUV, as well as its local fluid velocity $\mathbf{v}_{f_i}(t)$, constrained by the fact that the agents only have access to local information that they can obtain, be it through measurements or limited communication with their neighbors. In addition to the decentralized navigation approaches presented in this work, centralized solutions are presented as well, in order to establish a baseline for comparison with their decentralized alternatives.

3. Extended Kalman filter solutions

The most straightforward approach to the navigation problem is by using the measurements captured by the AUVs directly by employing an extended Kalman filter (EKF), which requires the linearization of the observation model Gelb (1974), Jazwinski (1970). Notice, however, that EKF-based solutions are usually not guaranteed to be globally convergent to the true solution and might require fine tuning of the filter parameters.

3.1. Centralized extended Kalman filter

While the centralized extended Kalman filter (CEKF) has access to all data, this comes with some serious drawbacks, such as heavy reliance on communication between AUVs and lack of scalability. In some cases, the implementation of a fully centralized approach can become very cumbersome or even unfeasible. Since all the data must be available at a single unit for computation, some information might need to be transmitted through long distances, thus resulting in the introduction of a delay into the system, which might not be easy to deal with. Regardless, centralized approaches have the potential to give the "best" estimates, and, as such, the CEKF is presented here for comparison with its decentralized counterpart, presented in Section 3.2.

3.1.1. Motion updates

Define the whole state as

$$\mathbf{x}[k] := \begin{bmatrix} \mathbf{x}_1[k] \\ \vdots \\ \mathbf{x}_N[k] \end{bmatrix} \in \mathbb{R}^{6N},$$

where each $\mathbf{x}_i$ is defined as in (3), representing the position and local fluid velocity of each AUV. Then, considering $\mathbf{A}$ and $\mathbf{B}$ as defined in (4) and (5), the complete system motion model is given by

$$\mathbf{x}[k+1] = \mathbf{A}_c\mathbf{x}[k] + \mathbf{B}_c\mathbf{u}[k] + \mathbf{w}[k],$$

where

$$\begin{cases} \mathbf{A}_c = \mathbf{I}_N \otimes \mathbf{A} \\ \mathbf{B}_c = \mathbf{I}_N \otimes \mathbf{B} \\ \mathbf{u}[k] = \begin{bmatrix} \mathbf{u}_1[k] \\ \vdots \\ \mathbf{u}_N[k] \end{bmatrix} \end{cases}, \tag{7}$$

where $N = |\mathcal{V}|$ is the number of agents, and $\mathbf{w}$ is the process noise. Notice here the presence of process noise, which accounts for unmodeled uncertainties. In this specific case, $\mathbf{u}$ is actually computed using sensor measurements, which are corrupted by noise. This can be modeled with the additional process noise term. Moreover, it can also be used to model slowly time-varying fluid velocities, considering a random walk model. The prediction step for the CEKF is given by

$$\begin{cases} \hat{\mathbf{x}}[k+1|k] = \mathbf{A}_c\hat{\mathbf{x}}[k] + \mathbf{B}_c\mathbf{u}[k] \\ \boldsymbol{\Sigma}[k+1|k] = \mathbf{A}_c\boldsymbol{\Sigma}[k|k]\mathbf{A}_c^T + \mathbf{Q}_c \end{cases},$$

where $\hat{\mathbf{x}}$ and $\boldsymbol{\Sigma}$ are the state estimate mean and covariance matrix, respectively, and $\mathbf{Q}_c$ is the centralized process noise covariance matrix. The process noise of each agent can be independently parameterized via $\mathbf{Q}_i$. Then, $\mathbf{Q}_c$ is obtained by concatenating the individual covariance matrices, as in $\mathbf{Q}_c = \operatorname{diag}(\mathbf{Q}_1, \ldots, \mathbf{Q}_N)$.

3.1.2. Measurement updates

In the following, the discrete-time dependence of the agents is omitted for clarity, unless explicitly needed. Let $\mathbf{y}_i = \mathbf{h}_i(\mathbf{x})$ be a measurement taken by an AUV with index i, and let the complete measurement vector, $\mathbf{y}$, be the concatenation of all the individual measurement vectors, as in

$$\mathbf{y} = \mathbf{h}(\mathbf{x}) = \begin{bmatrix} \mathbf{h}_1(\mathbf{x}) \\ \vdots \\ \mathbf{h}_N(\mathbf{x}) \end{bmatrix} + \mathbf{v}[k],$$

where $\mathbf{v}$ is the measurement noise. In order to perform the update step of the CEKF, the Jacobian of the measurement model must be computed according to

$$\mathbf{J}(\mathbf{x}) = \begin{bmatrix} \partial\mathbf{h}_1/\partial\mathbf{x} \\ \vdots \\ \partial\mathbf{h}_N/\partial\mathbf{x} \end{bmatrix} = \begin{bmatrix} \partial\mathbf{h}_1/\partial\mathbf{x}_1 & \cdots & \partial\mathbf{h}_1/\partial\mathbf{x}_N \\ \vdots & \ddots & \vdots \\ \partial\mathbf{h}_N/\partial\mathbf{x}_1 & \cdots & \partial\mathbf{h}_N/\partial\mathbf{x}_N \end{bmatrix}. \tag{8}$$

Since the real state is unknown, the Jacobian, $\mathbf{J} = \mathbf{J}(\mathbf{x})$, is approximated by $\hat{\mathbf{J}} = \mathbf{J}(\hat{\mathbf{x}})$, hence one of the reasons why a good enough initial state estimate is necessary.

Since EKF-based approaches allow for arbitrary measurement models, the general update equations are presented here, and some specific measurement models are described in the following section. Upon receiving measurements, the CEKF update equations are given by

$$\begin{cases} \hat{\mathbf{x}}[k+1|k+1] = \hat{\mathbf{x}}[k+1|k] + \mathbf{K}\left(\mathbf{y}[k+1] - \hat{\mathbf{y}}[k+1]\right) \\ \boldsymbol{\Sigma}[k+1|k+1] = \left(\mathbf{I}_{6N} - \mathbf{K}\hat{\mathbf{J}}\right)\boldsymbol{\Sigma}[k+1|k] \end{cases},$$

where

$$\mathbf{K} = \boldsymbol{\Sigma}[k+1|k]\hat{\mathbf{J}}^T\left(\hat{\mathbf{J}}\boldsymbol{\Sigma}[k+1|k]\hat{\mathbf{J}}^T + \mathbf{R}_c\right)^{-1}$$

is the Kalman gain, with $\hat{\mathbf{J}}$ evaluated using the predicted estimate, $\hat{\mathbf{x}}[k+1|k]$, and $\mathbf{R}_c$ is the centralized measurement vector noise covariance matrix. Lastly, $\hat{\mathbf{y}}[k+1] = \mathbf{h}(\hat{\mathbf{x}}[k+1|k])$ is the expected value of the measurement vector, given the current state estimate.

3.1.3. Measurement models

Some common measurement models will now be introduced. In particular, models for position, depth, and bearing measurements are presented. For ease of representation, the explicit discrete-time dependence is omitted unless explicitly necessary.

If the AUV making a measurement has direct access to position measurements $\mathbf{y}_i = \mathbf{h}_i(\mathbf{x}) = \mathbf{p}_i(t_k)$, its relevant part in (8) is given by

$$\frac{\partial\mathbf{h}_i}{\partial\mathbf{x}}(\mathbf{x}) = \begin{bmatrix} \cdots & \mathbf{I}_3 & \mathbf{0}_3 & \cdots \end{bmatrix},$$

where i is the index of the measuring agent and $\mathbf{I}_3$ occupies the columns corresponding to $\mathbf{p}_i$ in the complete state vector.

If the ith AUV takes bearing measurements about AUVs in its neighbor set, which, for simplicity, is assumed to be $\mathcal{N}_i = \{1, \ldots, |\mathcal{N}_i|\}$, in addition to a depth measurement about itself, $z_i(t_k) = \mathbf{p}_i^z(t_k)$, the measurement model is given by

$$\mathbf{h}_i(\mathbf{x}) = \begin{bmatrix} \mathbf{h}_{i1} \\ \vdots \\ \mathbf{h}_{i|\mathcal{N}_i|} \\ \mathbf{p}_i^z \end{bmatrix},$$

where

$$\mathbf{h}_{ij}(\mathbf{x}) = \mathbf{h}_b(\mathbf{p}_i, \mathbf{p}_j) = \begin{bmatrix} {}^{\mathcal{I}}\theta(\mathbf{p}_i, \mathbf{p}_j) \\ {}^{\mathcal{I}}\phi(\mathbf{p}_i, \mathbf{p}_j) \end{bmatrix}$$
$$= \begin{bmatrix} \operatorname{atan2}\left(\mathbf{p}_j^z - \mathbf{p}_i^z, \sqrt{(\mathbf{p}_j^x - \mathbf{p}_i^x)^2 + (\mathbf{p}_j^y - \mathbf{p}_i^y)^2}\right) \\ \operatorname{atan2}\left(\mathbf{p}_j^y - \mathbf{p}_i^y, \mathbf{p}_j^x - \mathbf{p}_i^x\right) \end{bmatrix},$$

and the angles ${}^{\mathcal{I}}\theta$ and ${}^{\mathcal{I}}\phi$ are represented in the inertial frame. Bearing measurements are measured in the AUV's body frame. However, the AUVs measure their orientation and, as such, can rotate the bearing measurement so that it is represented in $\{\mathcal{I}\}$. The Jacobian for the model $\mathbf{h}_i$ is given by

$$\frac{\partial\mathbf{h}_i}{\partial\mathbf{x}}(\mathbf{x}) = \begin{bmatrix} \partial\mathbf{h}_{i1}/\partial\mathbf{x} \\ \vdots \\ \partial\mathbf{h}_{i|\mathcal{N}_i|}/\partial\mathbf{x} \\ \mathbf{C}_z \end{bmatrix},$$

where

$$\frac{\partial\mathbf{h}_{ij}}{\partial\mathbf{x}}(\mathbf{x}) = \begin{bmatrix} \cdots & \mathbf{J}_{b_i}(\mathbf{x}) & \cdots & \mathbf{J}_{b_j}(\mathbf{x}) & \cdots \end{bmatrix},$$

with $\mathbf{J}_{b_i} := \partial\mathbf{h}_b/\partial\mathbf{x}_i$ and $\mathbf{J}_{b_j} := \partial\mathbf{h}_b/\partial\mathbf{x}_j$, and $\mathbf{C}_z \in \mathbb{R}^{1\times 6N}$ is such that all entries are zero except the one corresponding to $\mathbf{p}_i^z$ in the entire state vector.

While depth measurements are simple, geometrically, they remove a degree of freedom from the possible positions of the ith AUV, namely in the z direction. As such, coupling a depth measurement with a bearing measurement to another AUV will fix the possible positions of this agent to a single point, given the position of the jth AUV, and given that they do not lie on the same horizontal plane. The explicit expression of the bearing model Jacobian is omitted for brevity.

3.2. Decentralized extended Kalman filter

In this section, an implementation of the solution presented in Luft et al. (2018) is described for depth and bearing measurements, which will be labeled in this work as decentralized extended Kalman filter (DEKF). This asynchronous approach is completely decentralized and relies only on local communication between agents.

3.2.1. Motion model

The first insight behind this solution is that the cross-covariances between agents are only necessary when update steps happen. Because of this, if each agent can correctly update its cross-covariance to other agents without communicating with them, the motion update step of the Kalman filter presents no issue.

Consider the state of the ith agent, $\mathbf{x}_i$, defined as in (3), and denote its filtered estimate and covariance by $\hat{\mathbf{x}}_i$ and $\hat{\boldsymbol{\Sigma}}_{ii}$, respectively. Note that the DEKF approximates the CEKF, thus the covariances of each agent and their cross-covariances to other agents will not be exact, hence the chosen hat notation. Consider also the decomposition of the cross-covariance between agents i and j, $\hat{\boldsymbol{\Sigma}}_{ij}$, such that

$$\hat{\boldsymbol{\Sigma}}_{ij}[k] = \hat{\boldsymbol{\Phi}}_{ij}[k]\hat{\boldsymbol{\Phi}}_{ji}^T[k].$$

Let each agent carry its estimated belief, $\mathcal{B}_i := \{\hat{\mathbf{x}}_i, \hat{\boldsymbol{\Sigma}}_{ii}\}$, and cross-covariance factor, $\hat{\boldsymbol{\Phi}}_{ij}$, between itself and other agents it has knowledge of, i.e. $\hat{\boldsymbol{\Phi}}_{ij}$ for all $j \in \mathcal{N}_i$. The corresponding CEKF prediction equations for agent i, which account for its motion, are given by

$$\begin{cases} \hat{\mathbf{x}}_i[k+1|k] = \mathbf{A}\hat{\mathbf{x}}_i[k|k] + \mathbf{B}\mathbf{u}_i[k] \\ \boldsymbol{\Sigma}_{ii}[k+1|k] = \mathbf{A}\boldsymbol{\Sigma}_{ii}[k|k]\mathbf{A}^T + \mathbf{Q}_i \\ \boldsymbol{\Sigma}_{ij}[k+1|k] = \mathbf{A}\boldsymbol{\Sigma}_{ij}[k|k]\mathbf{A}^T \end{cases}, \tag{9}$$

and likewise for the agent with index j. So, if each AUV updates its cross-covariance factors to other AUVs through

$$\hat{\boldsymbol{\Phi}}_{ij}[k+1|k] = \mathbf{A}\hat{\boldsymbol{\Phi}}_{ij}[k|k] \;\forall j \in \mathcal{N}_i \tag{10}$$

when performing prediction steps, when they meet, their reconstructed cross-covariance is given by

$$\begin{aligned} \hat{\boldsymbol{\Sigma}}_{ij}[k+1|k] &= \mathbf{A}\hat{\boldsymbol{\Phi}}_{ij}[k|k]\hat{\boldsymbol{\Phi}}_{ji}[k|k]^T\mathbf{A}^T \\ &= \mathbf{A}\hat{\boldsymbol{\Sigma}}_{ij}[k|k]\mathbf{A}^T \\ &= \boldsymbol{\Sigma}_{ij}[k+1|k], \end{aligned}$$

if it holds that $\hat{\boldsymbol{\Sigma}}_{ij}[k|k] = \boldsymbol{\Sigma}_{ij}[k|k]$. In general, $\hat{\boldsymbol{\Sigma}}_{ij}[k|k] \neq \boldsymbol{\Sigma}_{ij}[k|k]$, however, what is important is that, since all terms are available, the prediction step of the CEKF can be reproduced exactly at each agent in a decentralized way while requiring no communication, thus resulting in no loss of estimation capabilities with respect to this step. All AUVs then predict their beliefs and cross-covariance factors to other agents according to (9) and (10), substituting $\mathbf{x}_i$ and $\boldsymbol{\Sigma}_{ii}$ by their estimated state and covariance matrix, $\hat{\mathbf{x}}_i$ and $\hat{\boldsymbol{\Sigma}}_{ii}$.

3.2.2. Observation model

A major difference should now be noted between the centralized and decentralized versions of this filter. While all the measurements are available simultaneously for computation of the update step in the CEKF, the DEKF is asynchronous and, as such, only one measurement vector is considered at a time. In a centralized approach, this would be equivalent to considering an observation model containing only one measurement at a time and performing several updates at each time step.

Consider that a leader AUV with index i takes a measurement, $\mathbf{y}_i$, of its position. Dropping the explicit discrete-time dependence, the measurement model for this agent is given by

$$\mathbf{h}(\mathbf{x}_i) = \begin{bmatrix}\mathbf{I}_3 & \mathbf{0}_3\end{bmatrix}\mathbf{x}_i = \mathbf{C}_i\mathbf{x}_i.$$

Since this equation only involves the measuring agent, the estimated belief and cross-covariance factors to other agents are updated according to

$$\begin{cases} \hat{\mathbf{x}}_i[k+1|k+1] = \hat{\mathbf{x}}_i[k+1|k] + \mathbf{K}_i(\mathbf{y}_i[k+1] - \hat{\mathbf{y}}_i[k+1]) \\ \hat{\boldsymbol{\Sigma}}_{ii}[k+1|k+1] = \left(\mathbf{I}_6 - \mathbf{K}_i\mathbf{C}_i\right)\hat{\boldsymbol{\Sigma}}_{ii}[k+1|k] \\ \hat{\boldsymbol{\Phi}}_{ij}[k+1|k+1] = \left(\mathbf{I}_6 - \mathbf{K}_i\mathbf{C}_i\right)\hat{\boldsymbol{\Phi}}_{ij}[k+1|k] \end{cases}, \tag{11}$$

where $\hat{\mathbf{y}}_i[k+1] = \mathbf{h}(\hat{\mathbf{x}}_i[k+1|k])$ is the expected measurement vector, $\mathbf{K}_i$ is the Kalman gain, given by

$$\mathbf{K}_i = \hat{\boldsymbol{\Sigma}}_{ii}[k+1|k]\mathbf{C}_i^T\left(\mathbf{C}_i\hat{\boldsymbol{\Sigma}}_{ii}[k+1|k]\mathbf{C}_i^T + \mathbf{R}_i\right)^{-1},$$

and $\mathbf{R}_i$ is the measurement noise covariance matrix. Note that the last equation of (11) should be performed for all agents that AUV i has knowledge of. In a centralized Kalman filter, measurements taken by an agent also affect the state of all agents that are correlated with it through previous measurements. However, in order to prevent excessive communication, the estimated beliefs of other agents are left unchanged.

Consider now the case where a follower AUV with index i takes a bearing measurement about another AUV with index j and a depth measurement about itself. Let $\hat{\mathbf{x}}_a$ be the joint estimate of the states, $\mathbf{x}_i$ and $\mathbf{x}_j$, and $\hat{\boldsymbol{\Sigma}}_{aa}$ its estimated covariance, such that

$$\hat{\mathbf{x}}_a[k] := \begin{bmatrix}\hat{\mathbf{x}}_i \\ \hat{\mathbf{x}}_j\end{bmatrix}, \quad \hat{\boldsymbol{\Sigma}}_{aa} := \begin{bmatrix}\hat{\boldsymbol{\Sigma}}_{ii} & \hat{\boldsymbol{\Sigma}}_{ij} \\ \hat{\boldsymbol{\Sigma}}_{ji} & \hat{\boldsymbol{\Sigma}}_{jj}\end{bmatrix}.$$

The update equations for the joint system are given by

$$\begin{cases} \hat{\mathbf{x}}_a[k+1|k+1] = \hat{\mathbf{x}}_a[k+1|k] + \mathbf{K}_a(\mathbf{y}_i[k+1] - \hat{\mathbf{y}}_i[k+1]) \\ \hat{\boldsymbol{\Sigma}}_{aa}[k+1|k+1] = \left(\mathbf{I}_6 - \mathbf{K}_a\hat{\mathbf{J}}_a\right)\hat{\boldsymbol{\Sigma}}_{aa}[k+1|k] \end{cases}, \tag{12}$$

where $\mathbf{y}_i[k+1]$ is the concatenation of the bearing measurement to another AUV with the captured depth measurement, $\hat{\mathbf{y}}_i[k+1]$ is its expected value, $\hat{\mathbf{J}}_a = \begin{bmatrix}\mathbf{J}_{f_i}(\hat{\mathbf{x}}_i, \hat{\mathbf{x}}_j) & \mathbf{J}_{f_j}(\hat{\mathbf{x}}_i, \hat{\mathbf{x}}_j)\end{bmatrix}$ is the Jacobian matrix of the joint system's measurement model computed using the predicted state estimates, $\hat{\mathbf{x}}_i[k+1|k]$ and $\hat{\mathbf{x}}_j[k+1|k]$, with $\mathbf{J}_{f_i}$ and $\mathbf{J}_{f_j}$ defined as

$$\begin{cases} \mathbf{J}_{f_i}(\mathbf{x}_i, \mathbf{x}_j) := \begin{bmatrix}\mathbf{J}_{b_i}(\mathbf{x}_i, \mathbf{x}_j) \\ \mathbf{C}_z\end{bmatrix} \\ \mathbf{J}_{f_j}(\mathbf{x}_i, \mathbf{x}_j) := \begin{bmatrix}\mathbf{J}_{b_j}(\mathbf{x}_i, \mathbf{x}_j) \\ \mathbf{0}_{1\times 6}\end{bmatrix} \end{cases},$$

and $\mathbf{K}_a$ is the Kalman gain, given by

$$\mathbf{K}_a = \hat{\boldsymbol{\Sigma}}_{aa}[k+1|k]\hat{\mathbf{J}}_a^T\left(\hat{\mathbf{J}}_a\hat{\boldsymbol{\Sigma}}_{aa}[k+1|k]\hat{\mathbf{J}}_a^T + \mathbf{R}_i\right)^{-1},$$

where $\mathbf{R}_i$ is the measurement noise covariance matrix. These quantities can be computed locally at the measuring agent, requiring only that AUV j transmits its estimated belief, $\mathcal{B}_j$, and its cross-covariance factor to agent i, $\hat{\boldsymbol{\Phi}}_{ji}$. AUV i is then responsible for reconstructing the joint system's belief and performing the joint update equations. It then communicates to AUV j its updated belief, obtained from the entries of $\hat{\mathbf{x}}_a[k+1|k+1]$ and $\hat{\boldsymbol{\Sigma}}_{aa}[k+1|k+1]$. In order not to double-count information, the cross-covariance between agents i and j must be distributed correctly. Since the decomposition of the cross-covariance between agents can be done in any way, it can be agreed beforehand, as done in Luft et al. (2018), that upon receiving updated estimates, agent j sets its cross-covariance factor to AUV i as the identity matrix, i.e. $\hat{\boldsymbol{\Phi}}_{ji}[k+1|k+1] = \mathbf{I}_6$, and AUV i sets

$$\hat{\boldsymbol{\Phi}}_{ij}[k+1|k+1] = \hat{\boldsymbol{\Sigma}}_{ij}[k+1|k+1], \tag{13}$$

where $\hat{\boldsymbol{\Sigma}}_{ij}[k+1|k+1]$ can be obtained from the updated joint state covariance matrix, $\hat{\boldsymbol{\Sigma}}_{aa}[k+1|k+1]$. This way, the cross-covariance between these two agents is preserved, since

$$\hat{\boldsymbol{\Phi}}_{ij}[k+1|k+1]\mathbf{I}_6^T = \hat{\boldsymbol{\Sigma}}_{ij}[k+1|k+1],$$

and there is no need for communicating to agent j a new cross-covariance factor. As before, in order to prevent communication between participating and non-participating agents, the state and covariance estimates of the latter are left unchanged.

The only terms that still need to tracked are the cross-covariance factors between participating and non-participating agents. This is stated to be the main contribution of the work in Luft et al. (2018) and, as such, only the main result is presented here. The interested reader is referred to the original work for details. The last update equation performed by participating agents is

$$\hat{\mathbf{\Phi}}_{il}[k+1|k+1] = \hat{\mathbf{\Sigma}}_{il}[k+1|k+1]\hat{\mathbf{\Sigma}}_{ii}^{-1}[k+1|k]\hat{\mathbf{\Phi}}_{il}[k+1|k], \tag{14}$$

where i represents the index of participating AUVs and l the index of non-participating agents. Note that both participating agents should perform the update (14).

To summarize, updates performed by leader AUVs when they take a measurement of their position are performed using (11). When an agent with index i takes a bearing measurement about AUV with index j, the updates are done using (12), (13), and (14), with AUV j setting $\hat{\mathbf{\Phi}}_{ji}[k+1|k+1] = \mathbf{I}_6$ upon receiving its updated belief, and performing (14) locally as well.

4. Artificial measurement solutions

An alternative to EKF-based filters is to construct artificial outputs such that the measurement model becomes linear, and then use this model to build an observer. With this approach, global convergence of the error to zero can be achieved depending on the measurement topology, increasing the time-efficiency of missions since an initial setup process is not required.

4.1. Independently interconnected Kalman filters

In this section, the approach considered in Santos et al. (2021) is presented. Briefly, it is based on constructing observers which present globally convergent error dynamics for each agent, and interconnecting them by using their estimates as "true" information, which is fed to the other observers. Because no cross-measurement information is kept between agents and each agent's estimate is taken as true information by other agents, this estimator achieves the worst performance out of the considered ones, though it does achieve globally convergent dynamics, provided that each agent's observer is globally observable, and the information flow is unidirectional, as is the case for tiered formations (Santos et al., 2021; Viegas et al., 2016).

The prediction and update equations for each agent's observer follow the general Kalman filter dynamics. Letting $\hat{\mathbf{x}}_i$ and $\mathbf{\Sigma}_{ii}$ be the state estimate and covariance of the ith AUV, respectively, the prediction step equations are given by

$$\begin{cases} \hat{\mathbf{x}}_i[k+1|k] = \mathbf{A}\hat{\mathbf{x}}[k|k] + \mathbf{B}\mathbf{u}_i[k] \\ \mathbf{\Sigma}_{ii}[k+1|k] = \mathbf{A}\mathbf{\Sigma}_{ii}[k|k]\mathbf{A}^T + \mathbf{Q}_i \end{cases},$$

where $\mathbf{Q}_i$ is the process noise covariance matrix of the agent. Likewise, the update equations are

$$\begin{cases} \hat{\mathbf{x}}_i[k+1|k+1] = \hat{\mathbf{x}}_i[k+1|k] + \mathbf{K}_i(\mathbf{y}_i[k+1] - \mathbf{C}_i\hat{\mathbf{x}}_i[k+1|k]) \\ \mathbf{\Sigma}_{ii}[k+1|k+1] = \left(\mathbf{I}_6 - \mathbf{K}_i\mathbf{C}_i\right)\mathbf{\Sigma}_{ii}[k+1|k] \end{cases},$$

where $\mathbf{C}_i$ is the observation matrix to be described in the following, $\mathbf{y}_i[k+1]$ is the observation vector, constructed using measurements obtained at time $t = t_{k+1}$, and

$$\mathbf{K}_i = \mathbf{\Sigma}_{ii}[k+1|k]\mathbf{C}_i^T\left(\mathbf{C}_i\mathbf{\Sigma}_{ii}[k+1|k]\mathbf{C}_i^T + \mathbf{R}_i\right)^{-1}$$

is the Kalman gain, where $\mathbf{R}_i$ is a suitable measurement noise covariance matrix.

Assuming that the ith AUV is a leader, then it has direct access to position measurements, such that $\mathbf{y}_i[k+1]$ is its position measurement vector, and $\mathbf{C}_i = \begin{bmatrix}\mathbf{I}_3 & \mathbf{0}_3\end{bmatrix}$. If, instead, the ith agent is a follower AUV which successfully obtains bearing measurements about its neighbors, $j \in \mathcal{N}_i$, and its depth, it then has access to $z_i = \mathbf{p}_i^z(t_{k+1})$ and $\mathbf{d}_{ij}(t_{k+1})$ for all $j \in \mathcal{N}_i$, computed from the obtained bearing angles, θ_{ij} and ϕ_{ij}, according to (6). In the following, it is assumed, for ease of representation and without loss of generality, that $\mathcal{N}_i = \{1, \dots, |\mathcal{N}_i|\}$.

Upon building the direction vector, the projection matrix,

$$\mathbf{D}_{ij}(t_k) := \mathbf{d}_{ij}(t_k)\mathbf{d}_{ij}^T(t_k), \tag{15}$$

and its orthogonal complement,

$$\bar{\mathbf{D}}_{ij}(t_k) := \mathbf{I}_3 - \mathbf{d}_{ij}(t_k)\mathbf{d}_{ij}^T(t_k), \tag{16}$$

are constructed and the following equality holds,

$$\bar{\mathbf{D}}_{ij}(t_k)\mathbf{p}_i(t_k) = \bar{\mathbf{D}}_{ij}(t_k)\mathbf{p}_j(t_k).$$

Since the true positions of the neighboring AUVs are unknown, the observation vector of the ith AUV, considering also its depth measurement, is defined as

$$\mathbf{y}_i[k+1] := \begin{bmatrix} \bar{\mathbf{D}}_{i1}(t_{k+1})\hat{\mathbf{p}}_1(t_{k+1}|t_k) \\ \vdots \\ \bar{\mathbf{D}}_{i|\mathcal{N}_i|}(t_{k+1})\hat{\mathbf{p}}_{|\mathcal{N}_i|}(t_{k+1}|t_k) \\ z_i(t_{k+1}) \end{bmatrix},$$

where $\hat{\mathbf{p}}_j(t_{k+1}|t_k)$ is the predicted position estimate of the jth agent, extracted from $\hat{\mathbf{x}}_j[k+1|k]$, and z_i is the depth measurement obtained by the ith agent. Likewise, the observation matrix is defined as

$$\mathbf{C}_i := \begin{bmatrix} \bar{\mathbf{D}}_{i1}(t_{k+1}) & \mathbf{0}_3 \\ \vdots & \\ \bar{\mathbf{D}}_{i|\mathcal{N}_i|}(t_{k+1}) & \mathbf{0}_3 \\ \mathbf{e}_z & \mathbf{0}_{1\times 3} \end{bmatrix},$$

where $\mathbf{e}_z = \begin{bmatrix}0 & 0 & 1\end{bmatrix}$.

In Santos et al. (2021), an observer such as this one is considered for the case of acyclical formations, where it is shown that it exhibits globally exponentially stable error dynamics, provided that the leader agents also present this kind of error dynamics. If cycles are introduced into the measurement graph, there will be a reintroduction of the estimation errors into some of the agents, which raises some questions about the convergence of the proposed observer. The performance of this filter under a cyclical measurement topology is analyzed via Monte Carlo simulations in Section 5.

4.2. Centralized observer

The centralized version of the observers based on bearing and depth measurements is presented in this section. Again, a centralized approach might not be feasible in practice, but it serves as a baseline for comparison with the decentralized approaches studied in this work.

Let the state of the centralized system be defined as

$$\mathbf{x}[k] := \begin{bmatrix} \mathbf{x}_1[k] \\ \vdots \\ \mathbf{x}_N[k] \end{bmatrix} \in \mathbb{R}^{6N}$$

and let $\hat{\mathbf{x}}$ and $\mathbf{\Sigma}$ be its state estimate and covariance matrix, respectively. The motion model of this approach is the same as that of the CEKF, i.e., upon receiving the control signals, the agents' estimates are predicted according to

$$\begin{cases} \hat{\mathbf{x}}[k+1|k] = \mathbf{A}_c\hat{\mathbf{x}}[k|k] + \mathbf{B}_c\mathbf{u}[k] \\ \mathbf{\Sigma}[k+1|k] = \mathbf{A}_c\mathbf{\Sigma}[k|k]\mathbf{A}_c^T + \mathbf{Q}_c \end{cases},$$

where $\mathbf{A}_c$ and $\mathbf{B}_c$ are defined as in (7) and $\mathbf{Q}_c$ is the centralized process noise covariance matrix.

Let $\mathbf{y}$ and $\mathbf{C}_c$ be the complete measurement vector and centralized observation matrix, respectively, such that $\mathbf{y}[k] = \mathbf{C}_c\mathbf{x}[k]$. Let $\mathbf{y}$ be composed of individual agent measurement vectors, such that

$$\mathbf{y} := \begin{bmatrix} \mathbf{y}_1 \\ \vdots \\ \mathbf{y}_N \end{bmatrix}, \quad \mathbf{C}_c := \begin{bmatrix} \mathbf{C}_1 \\ \vdots \\ \mathbf{C}_N \end{bmatrix}$$

where $\mathbf{y}_i$ is the measurement vector captured by agent i, and $\mathbf{C}_i$ is its measurement model. For the case of leader agents, $\mathbf{y}_i$ is a position

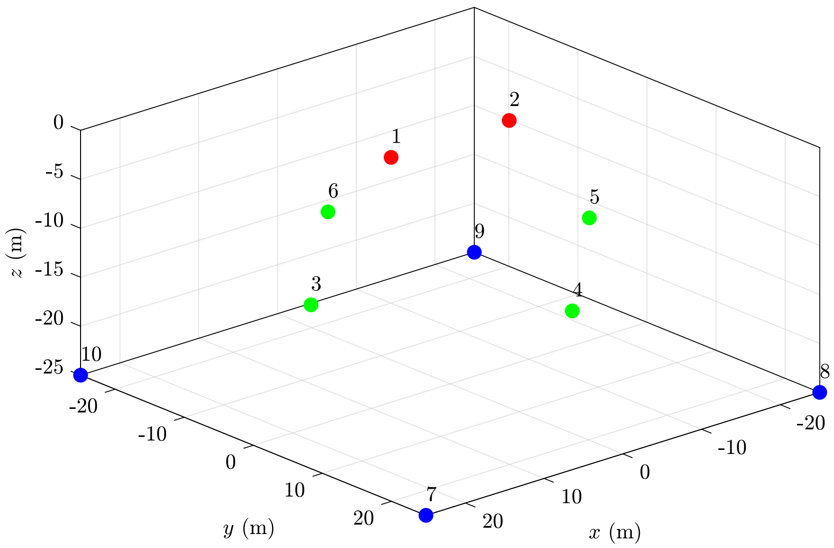

(a) Initial spatial configuration, which the agents maintain for the first half of the mission.

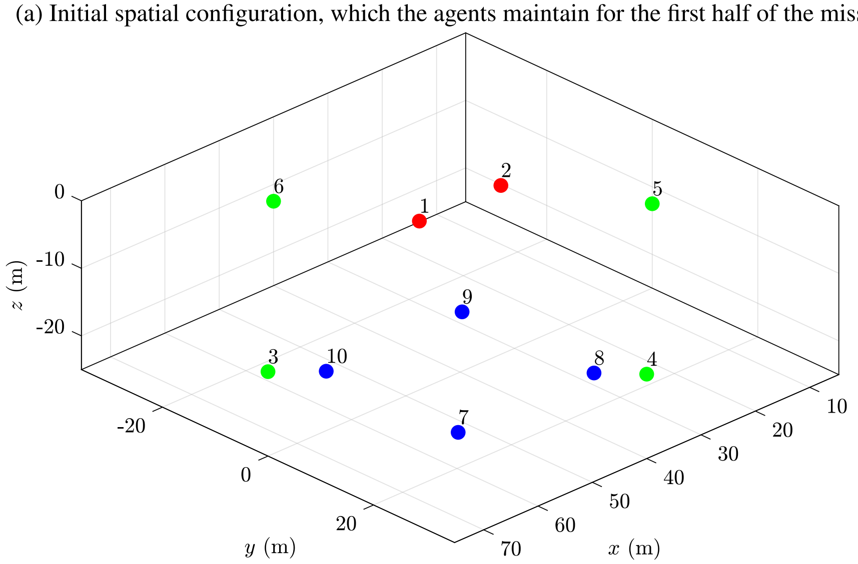

(b) Second spatial configuration, which the agents change to at around $t = 400$ s.

Fig. 2. Spatial configurations maintained by the agents throughout the mission.

measurement and $\mathbf{C}_i = \begin{bmatrix}\cdots & \mathbf{I}_3 & \mathbf{0}_3 & \cdots\end{bmatrix}$. As for follower AUVs, considering the relationship presented in Santos et al. (2021),

$$\bar{\mathbf{D}}_{ij}(t_k)(\mathbf{p}_i(t_k) - \mathbf{p}_j(t_k)) = \mathbf{0}_{3\times 1},$$

and that the AUV has access to depth measurements, the measurement vector, at time $t = t_{k+1}$ is then given by

$$\mathbf{y}_i[k+1] = \begin{bmatrix}\mathbf{0}_{3|\mathcal{N}_i|\times 1} \\ z_i(t_{k+1})\end{bmatrix},$$

where z_i is the depth measurement. Each $\mathbf{C}_i$ relates the measurements captured by the ith agent with the total state vector using the orthogonal complement of the bearing projection matrix and depth information, as shown below, in Example 2.

The total state estimate is then corrected according to the standard Kalman filter update equations

$$\begin{cases}\hat{\mathbf{x}}[k+1|k+1] = \hat{\mathbf{x}}[k+1|k] + \mathbf{K}(\mathbf{y}[k+1] - \mathbf{C}_c\hat{\mathbf{x}}[k+1|k]) \\ \boldsymbol{\Sigma}[k+1|k+1] = \left(\mathbf{I} - \mathbf{K}\mathbf{C}_c\right)\boldsymbol{\Sigma}[k+1|k]\end{cases},$$

where $\mathbf{K} = \boldsymbol{\Sigma}[k+1|k]\mathbf{C}_c^T\left(\mathbf{C}_c\boldsymbol{\Sigma}[k+1|k]\mathbf{C}_c^T + \mathbf{R}_c\right)^{-1}$ is the Kalman gain, with $\mathbf{R}_c$ the total observation vector noise covariance matrix.

Example 2. Considering the formation presented in Fig. 1, the observation matrix of each agent is given by

$$\mathbf{C}_1 = \begin{bmatrix}\mathbf{I}_3 & \mathbf{0}_3 & \mathbf{0}_3 & \mathbf{0}_3 & \mathbf{0}_3 & \mathbf{0}_3\end{bmatrix},$$

$$\mathbf{C}_2 = \begin{bmatrix}-\bar{\mathbf{D}}_{21} & \mathbf{0}_3 & \bar{\mathbf{D}}_{21} & \mathbf{0}_3 & \mathbf{0}_3 & \mathbf{0}_3 \\ \mathbf{0}_3 & \mathbf{0}_3 & \bar{\mathbf{D}}_{23} & \mathbf{0}_3 & -\bar{\mathbf{D}}_{23} & \mathbf{0}_3 \\ \mathbf{0}_{1\times 3} & \mathbf{0}_{1\times 3} & \mathbf{e}_z & \mathbf{0}_{1\times 3} & \mathbf{0}_{1\times 3} & \mathbf{0}_{1\times 3}\end{bmatrix},$$

$$\mathbf{C}_3 = \begin{bmatrix}-\bar{\mathbf{D}}_{31} & \mathbf{0}_3 & \mathbf{0}_3 & \mathbf{0}_3 & \bar{\mathbf{D}}_{31} & \mathbf{0}_3 \\ \mathbf{0}_3 & \mathbf{0}_3 & -\bar{\mathbf{D}}_{32} & \mathbf{0}_3 & \bar{\mathbf{D}}_{32} & \mathbf{0}_3 \\ \mathbf{0}_{1\times 3} & \mathbf{0}_{1\times 3} & \mathbf{0}_{1\times 3} & \mathbf{0}_{1\times 3} & \mathbf{e}_z & \mathbf{0}_{1\times 3}\end{bmatrix},$$

where the $\mathbf{D}_{ij}$ matrices are computed using the quantities obtained at time $t = t_{k+1}$, though the explicit time dependence was omitted due to space limitations. The centralized observation matrix is then given by

$$\mathbf{C}_c = \begin{bmatrix}\mathbf{I}_3 & \mathbf{0}_3 & \mathbf{0}_3 & \mathbf{0}_3 & \mathbf{0}_3 & \mathbf{0}_3 \\ -\bar{\mathbf{D}}_{21} & \mathbf{0}_3 & \bar{\mathbf{D}}_{21} & \mathbf{0}_3 & \mathbf{0}_3 & \mathbf{0}_3 \\ \mathbf{0}_3 & \mathbf{0}_3 & \bar{\mathbf{D}}_{23} & \mathbf{0}_3 & -\bar{\mathbf{D}}_{23} & \mathbf{0}_3 \\ \mathbf{0}_{1\times 3} & \mathbf{0}_{1\times 3} & \mathbf{e}_z & \mathbf{0}_{1\times 3} & \mathbf{0}_{1\times 3} & \mathbf{0}_{1\times 3} \\ -\bar{\mathbf{D}}_{31} & \mathbf{0}_3 & \mathbf{0}_3 & \mathbf{0}_3 & \bar{\mathbf{D}}_{31} & \mathbf{0}_3 \\ \mathbf{0}_3 & \mathbf{0}_3 & -\bar{\mathbf{D}}_{32} & \mathbf{0}_3 & \bar{\mathbf{D}}_{32} & \mathbf{0}_3 \\ \mathbf{0}_{1\times 3} & \mathbf{0}_{1\times 3} & \mathbf{0}_{1\times 3} & \mathbf{0}_{1\times 3} & \mathbf{e}_z & \mathbf{0}_{1\times 3}\end{bmatrix},$$

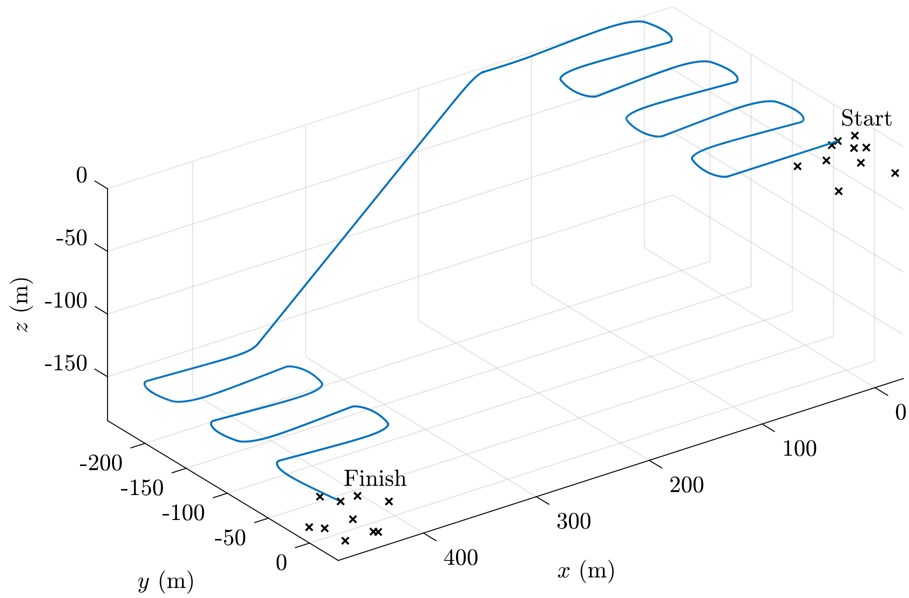

Fig. 3. Nominal trajectory of the leader agent with index 1.

and the measurement vector, in this example, is given by

$$\mathbf{y}[k+1] = \begin{bmatrix} \mathbf{y}_1[k+1] \\ \mathbf{0}_{6\times 1} \\ z_2(t_{k+1}) \\ \mathbf{0}_{6\times 1} \\ z_3(t_{k+1}) \end{bmatrix},$$

where $\mathbf{y}_1[k+1]$ is the position measurement obtained by the leader AUV with index 1 and z_2, z_3 are the depth measurements obtained by agents 2 and 3, respectively.

4.3. Decentralized observer

The algorithm presented in this section is based on a slight extension of the distributed filter presented in Section 3.2, which allows for asynchronous updates involving more than two agents at a time, at the cost of extra communication. Similarly to the DEKF, each agent carries its own estimated belief, $\mathcal{B}_i = \{\hat{\mathbf{x}}_i, \hat{\boldsymbol{\Sigma}}_{ii}\}$, and cross-covariance factors to other AUVs, $\hat{\boldsymbol{\Phi}}_{ij}$. The prediction equations for these quantities are performed as in the DEKF. In fact, the only difference between these two approaches is the update step, which is not restricted to pairwise communication and uses the projection matrix (16) introduced in Santos et al. (2021).

The update equations for leader agents are the exact same as in the DEKF approach, including the cross-covariance factor updates. As for relative measurements, let a follower agent with index i take bearing measurements about its neighbors, which will be assumed, without loss of generality, to have indices $j \in \mathcal{N}_i = \{1, \ldots, |\mathcal{N}_i|\}$, and a depth measurement about itself. Since $\bar{\mathbf{D}}_{ij}(t_k)(\mathbf{p}_i(t_k) - \mathbf{p}_j(t_k)) = \mathbf{0}_{3\times 1}$, then, considering the joint state vector

$$\mathbf{x}_a[k] := \begin{bmatrix} \mathbf{x}_i[k] \\ \mathbf{x}_1[k] \\ \vdots \\ \mathbf{x}_{|\mathcal{N}_i|}[k] \end{bmatrix},$$

where $\mathbf{x}_i$ is the state of the measuring agent, one has

$$\mathbf{y}_a[k+1] := \begin{bmatrix} \mathbf{0}_{3\times|\mathcal{N}_i|} \\ z_i(t_{k+1}) \end{bmatrix} = \mathbf{C}_a \mathbf{x}_a[k+1],$$

where

$$\mathbf{C}_a = \begin{bmatrix} \bar{\mathbf{D}}_{i1} & \mathbf{0}_{3\times 3} & -\bar{\mathbf{D}}_{i1} & \mathbf{0}_{3\times 3} & \cdots & \mathbf{0}_{3\times 3} & \mathbf{0}_{3\times 3} \\ \vdots & \vdots & \vdots & \vdots & \ddots & \vdots & \vdots \\ \bar{\mathbf{D}}_{i|\mathcal{N}_i|} & \mathbf{0}_{3\times 3} & \mathbf{0}_{3\times 3} & \mathbf{0}_{3\times 3} & \cdots & -\bar{\mathbf{D}}_{i|\mathcal{N}_i|} & \mathbf{0}_{3\times 3} \\ \mathbf{e}_z^T & \mathbf{0}_{1\times 3} & \mathbf{0}_{1\times 3} & \mathbf{0}_{1\times 3} & \cdots & \mathbf{0}_{1\times 3} & \mathbf{0}_{1\times 3} \end{bmatrix},$$

and z_i is the depth measurement of the measuring agent. Note that the matrices $\bar{\mathbf{D}}_{ij}$ are, again, computed using the quantities obtained at time $t = t_{k+1}$, such that, when computing the update equations, one has $\bar{\mathbf{D}}_{ij} = \bar{\mathbf{D}}_{ij}(t_{k+1})$.

Let the estimate of the joint system's state, composed of the AUVs participating in the measurement of agent i, be denoted as $\hat{\mathbf{x}}_a$, and its associated covariance matrix estimate as

$$\hat{\boldsymbol{\Sigma}}_{aa} = \begin{bmatrix} \hat{\boldsymbol{\Sigma}}_{ii} & \hat{\boldsymbol{\Sigma}}_{i1} & \cdots & \hat{\boldsymbol{\Sigma}}_{i|\mathcal{N}_i|} \\ \hat{\boldsymbol{\Sigma}}_{1i} & \hat{\boldsymbol{\Sigma}}_{11} & \cdots & \hat{\boldsymbol{\Sigma}}_{1|\mathcal{N}_i|} \\ \vdots & \vdots & \ddots & \vdots \\ \hat{\boldsymbol{\Sigma}}_{|\mathcal{N}_i|i} & \hat{\boldsymbol{\Sigma}}_{|\mathcal{N}_i|1} & \cdots & \hat{\boldsymbol{\Sigma}}_{|\mathcal{N}_i||\mathcal{N}_i|} \end{bmatrix}, \tag{17}$$

where the discrete-time dependence was also dropped for readability. In order to reduce the required amount of communication, the cross-covariance terms between the neighbors of AUV i can be ignored, such that

$$\hat{\boldsymbol{\Sigma}}_{aa} \approx \begin{bmatrix} \hat{\boldsymbol{\Sigma}}_{ii} & \hat{\boldsymbol{\Sigma}}_{i1} & \cdots & \hat{\boldsymbol{\Sigma}}_{i|\mathcal{N}_i|} \\ \hat{\boldsymbol{\Sigma}}_{1i} & \hat{\boldsymbol{\Sigma}}_{11} & \cdots & \mathbf{0}_{3\times 3} \\ \vdots & \vdots & \ddots & \vdots \\ \hat{\boldsymbol{\Sigma}}_{|\mathcal{N}_i|i} & \mathbf{0}_{3\times 3} & \cdots & \hat{\boldsymbol{\Sigma}}_{|\mathcal{N}_i||\mathcal{N}_i|} \end{bmatrix}.$$

If the communication restrictions are not as strict, the cross-covariance terms $\hat{\boldsymbol{\Sigma}}_{jk}$, for $j, k \in \mathcal{N}_i$, can be obtained from the cross-covariance factors that the participating agents j and k carry, by letting them communicate these quantities to agent i, which can then reconstruct the cross-covariance term and place it into $\hat{\boldsymbol{\Sigma}}_{aa}$. For follower AUVs, the Kalman gain is computed for the joint system using the reconstructed covariance matrix, such that

$$\mathbf{K}_a = \hat{\boldsymbol{\Sigma}}_{aa}[k+1|k]\mathbf{C}_a^T \left(\mathbf{C}_a \hat{\boldsymbol{\Sigma}}_{aa}[k+1|k]\mathbf{C}_a^T + \mathbf{R}_a \right)^{-1},$$

where $\mathbf{R}_a$ is a compatible measurement noise covariance matrix. The new beliefs are then computed using the standard Kalman filter update equations

$$\begin{cases} \hat{\mathbf{x}}_a[k+1|k+1] = \hat{\mathbf{x}}_a[k+1|k] + \mathbf{K}_a(\mathbf{y}_a[k+1] - \mathbf{C}_a \hat{\mathbf{x}}_a[k+1|k]) \\ \hat{\boldsymbol{\Sigma}}_{aa}[k+1|k+1] = \left(\mathbf{I}_6 - \mathbf{K}_a \mathbf{C}_a\right) \hat{\boldsymbol{\Sigma}}_{aa}[k+1|k] \end{cases},$$

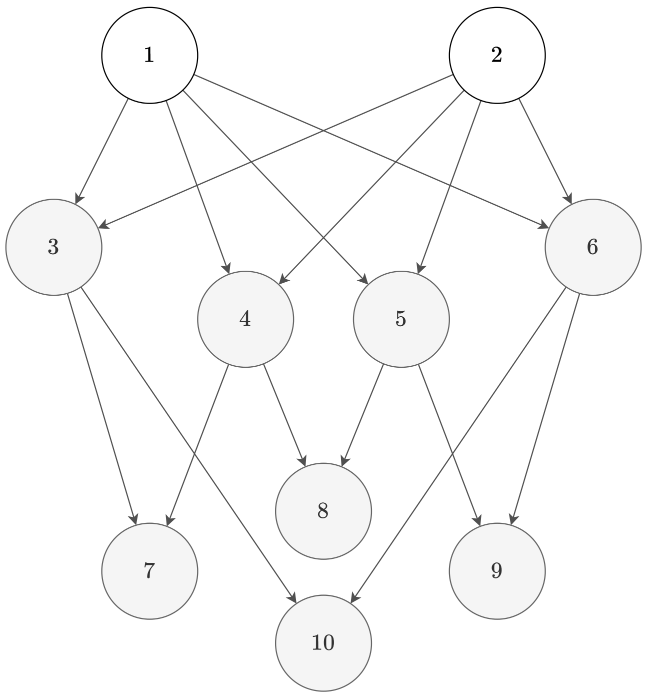

(a) Acyclical topology measurement graph.

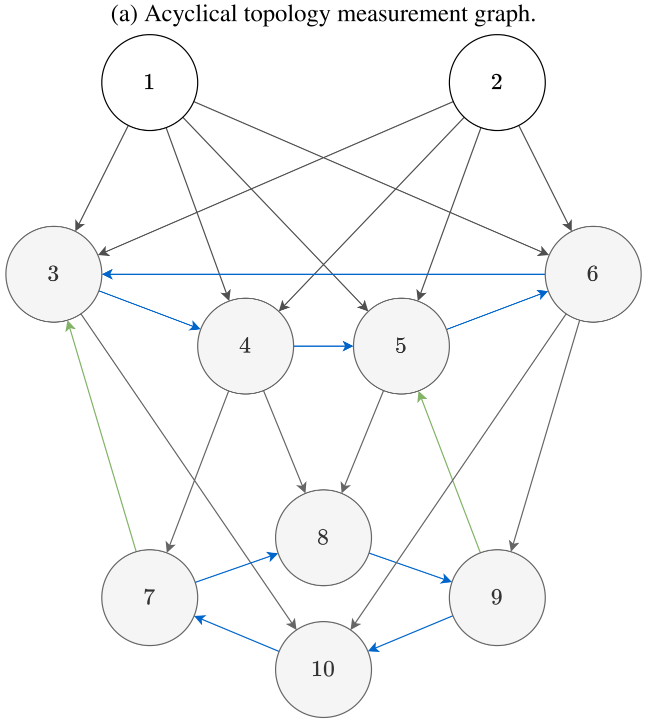

(b) Cyclical topology measurement graph.

Fig. 4. Measurement topologies.

and then communicated to the participating agents. In turn, these agents update their cross-covariance factors to non-participating ones according to the approximation presented in Luft et al. (2018), i.e.,

$$\hat{\mathbf{\Phi}}_{ik}[k+1|k+1] = \hat{\mathbf{\Sigma}}_{aa}[k+1|k+1]\hat{\mathbf{\Sigma}}_{aa}^{-1}[k+1|k]\hat{\mathbf{\Phi}}_{ik}[k+1|k],$$

for every non-participating agent with index k that they have knowledge of. In case the full covariance matrix was used, the new cross-covariance terms between the participating agents can be factorized and distributed in a way that does not double-count information. A possible rule for distributing the cross-covariance terms could be, for example

$$\hat{\mathbf{\Phi}}_{ij}[k+1|k+1] = \begin{cases} \hat{\mathbf{\Sigma}}_{ij}[k+1] & \text{if } i < j \\ \mathbf{I}_6 & \text{if } i > j \end{cases},$$

though it is not necessarily the one which minimizes the amount of communication.

4.4. Static-gain decentralized observer

In this section, a technique for computing steady-state observer gains for agents that can acquire relative position measurements to their neighbors, presented in Viegas et al. (2018), is briefly described. Local observers for each follower agent are then designed, coupling these gains with an artificial relative position output built from bearing measurements and depth differences between agents. Each observer has a prediction step and an update step, as with regular Kalman filters, though a covariance matrix is not maintained.

All agents predict their estimate according to

$$\hat{\mathbf{x}}_i[k+1|k] = \mathbf{A}\hat{\mathbf{x}}_i[k|k] + \mathbf{B}\mathbf{u}_i[k],$$

where $\mathbf{A}$, $\mathbf{B}$, and $\mathbf{u}_i[k]$ are defined as in (4), (5), and (2), respectively. Upon taking measurements and predicting its state, the ith agent updates its estimate according to

$$\hat{\mathbf{x}}_i[k+1|k+1] = \begin{cases} \hat{\mathbf{x}}_i[k+1|k] + \mathbf{K}_i(\mathbf{y}_i[k+1] - \hat{\mathbf{x}}_i[k+1|k]) & \text{if } i \in \mathcal{V}_L \\ \hat{\mathbf{x}}_i[k+1|k] + \mathbf{K}_i(\mathbf{m}_i[k+1] - \Delta\hat{\mathbf{x}}[k+1|k]) & \text{if } i \in \mathcal{V}_F \end{cases},$$

where

$$\Delta\hat{\mathbf{x}} = \begin{bmatrix} \hat{\mathbf{x}}_i[k+1|k] - \hat{\mathbf{x}}_1[k+1|k] \\ \vdots \\ \hat{\mathbf{x}}_i[k+1|k] - \hat{\mathbf{x}}_{|\mathcal{N}_i|}[k+1|k] \\ \hat{\mathbf{p}}_i^z(t_{k+1}|t_k) \end{bmatrix},$$

$\mathbf{y}_i[k+1]$ is an absolute position measurement, and $\mathbf{m}_i[k+1]$ is a vector containing the captured depth measurement and relative position measurements between the measuring agent and its neighbors, assumed to be $\mathcal{N}_i = \{1,\ldots,|\mathcal{N}_i|\}$. The formation gains, $\mathbf{K}_i$, are computed by propagating the centralized system's covariance prediction and update equations using a gain matrix computed subject to a certain sparsity constraint, which, in this case, constrains the total system gain matrix, $\mathbf{K}$, to be block diagonal. Upon computing the formation gains, each block of $\mathbf{K}$ is extracted and set as $\mathbf{K}_i$ accordingly.

The centralized system's motion model is identical to that of the CEKF, presented in Section 3.1.1, such that $\mathbf{A}_c = \mathbf{I}_N \otimes \mathbf{A}$. As for the observation model, whereas leader agents can capture measurements of their own position, follower agents can only capture relative position and depth measurements, that is

$$\mathbf{m}_i[k+1] = \begin{bmatrix} \mathbf{p}_i(t_{k+1}) - \mathbf{p}_1(t_{k+1}) \\ \vdots \\ \mathbf{p}_i(t_{k+1}) - \mathbf{p}_{|\mathcal{N}_i|}(t_{k+1}) \\ z_i(t_{k+1}) \end{bmatrix}.$$

Let $\mathbf{C}_c$ be centralized system's observation matrix, containing matrices $\mathbf{C}_L = \begin{bmatrix}\mathbf{I}_3 & \mathbf{0}_3\end{bmatrix}$ for leader measurement entries. For follower measurement entries, the measuring agent's entry is modeled with $\mathbf{C}_L$, whereas the entry corresponding to the agent whose measurement is taken about is modeled with $-\mathbf{C}_L$. Additionally, the depth measurements taken by follower agents are modeled using the vector $\mathbf{e}_z = \begin{bmatrix}0 & 0 & 1 & 0 & 0 & 0\end{bmatrix}$. This construction is exemplified in Example 3.

Following the results derived in Viegas et al. (2018), the centralized gain subject to a sparsity constraint is then computed by propagating

$$\mathbf{\Sigma}[k+1|k] = \mathbf{A}_c\mathbf{\Sigma}[k|k]\mathbf{A}_c^T + \mathbf{Q}_c \tag{18}$$

and

$$\mathbf{\Sigma}[k+1|k+1] = \quad (\mathbf{I}_{6N} - \mathbf{K}[k]\mathbf{C}_c)\mathbf{\Sigma}[k+1|k](\mathbf{I}_{6N} - \mathbf{K}[k]\mathbf{C}_c)^T$$

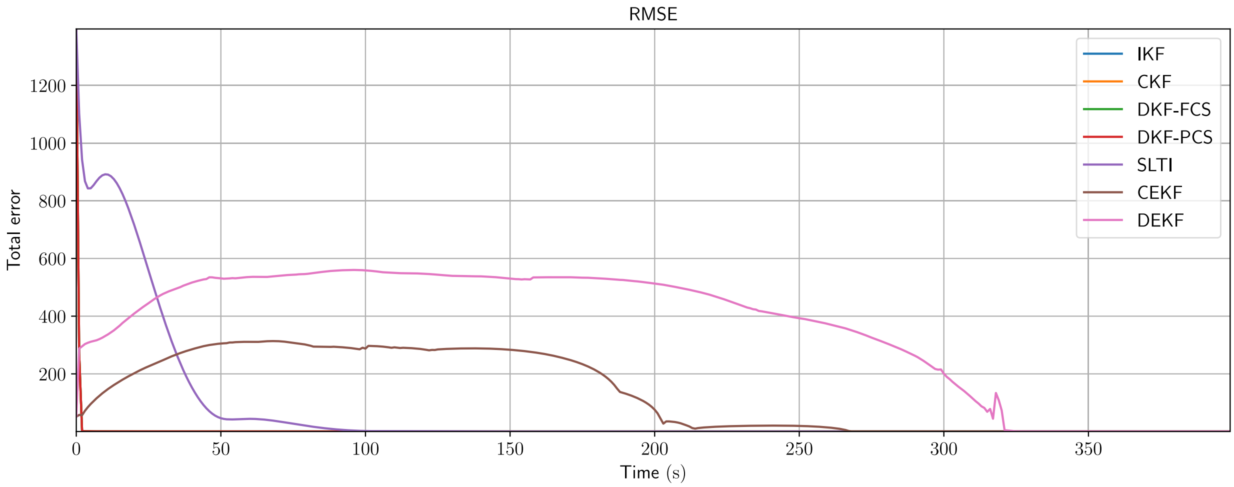

(a) Acyclical topology RMSE results of observers tuned for convergence speed.

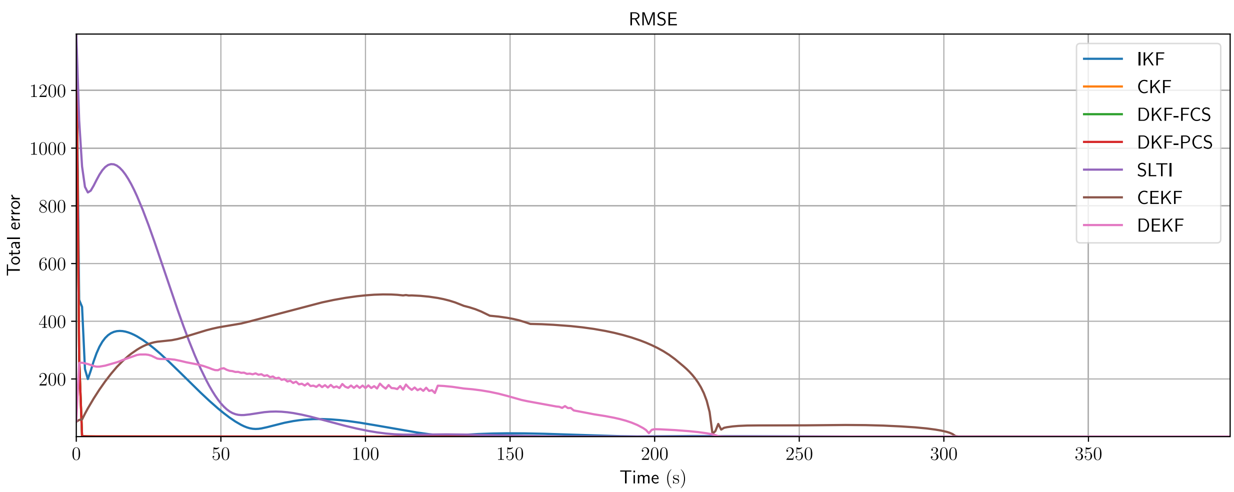

(b) Cyclical topology RMSE results of observers tuned for convergence speed.

Fig. 5. RMSE results.

$$+\ \mathbf{K}[k]\mathbf{R}_c\mathbf{K}[k]^T \tag{19}$$

until the trace of $\boldsymbol{\Sigma}[k+1|k+1]$ reaches a steady-state value. Define $\mathbf{l}_i \in \mathbb{R}^{6N}$ as the unit vector such that all entries are zero except the ith one and let $\mathbf{L}_i := \mathrm{diag}(\mathbf{l}_i)$. In the above equations, $\mathbf{Q}_c = \mathrm{diag}(\mathbf{Q}_1,\dots,\mathbf{Q}_N)$ is the centralized process noise covariance matrix, $\mathbf{R}_c$ is the centralized observation model noise covariance matrix, and $\mathbf{K}[k]$ is given by

$$\mathbf{K}[k] = \sum_{i=1}^{6N} \mathbf{L}_i\boldsymbol{\Sigma}[k+1|k]\mathbf{C}_c^T\mathbf{M}_i\left(\mathbf{I}_{6N} - \mathbf{M}_i + \mathbf{M}_i\mathbf{S}\mathbf{M}_i\right)^{-1},$$

where

$$\mathbf{S} = \mathbf{C}_c\boldsymbol{\Sigma}[k+1|k]\mathbf{C}_c^T + \mathbf{R}_c.$$

The sparsity constraint is imposed by the matrix $\mathbf{M}_i$, which is built to encode the measurements each agent has access to. Letting $\mathbf{s}_i$ be a vector such that

$$\begin{cases} \mathbf{s}_i^j = 1 & \text{if } \mathbf{E}^{ij} = 1 \\ \mathbf{s}_i^j = 0 & \text{otherwise} \end{cases},$$

where $\mathbf{E} \in \mathbb{R}^{6N\times m}$ is the sparsity pattern matrix, with m the total measurement vector length, $\mathbf{M}_i$ is then built as $\mathbf{M}_i = \mathrm{diag}(\mathbf{s}_i)$.

Example 3. Consider again the formation presented in Fig. 1. Following the measurement ordering adopted in Example 2, the centralized observation matrix, $\mathbf{C}_c$, is given by

$$\mathbf{C}_c = \begin{bmatrix} \mathbf{C}_L & \mathbf{0}_{3\times6} & \mathbf{0}_{3\times6} \\ -\mathbf{C}_L & \mathbf{C}_L & \mathbf{0}_{3\times6} \\ \mathbf{0}_{1\times6} & \mathbf{e}_z & \mathbf{0}_{1\times6} \\ -\mathbf{C}_L & \mathbf{0}_{3\times6} & \mathbf{C}_L \\ \mathbf{0}_{3\times6} & -\mathbf{C}_L & \mathbf{C}_L \\ \mathbf{0}_{1\times6} & \mathbf{0}_{1\times6} & \mathbf{e}_z \end{bmatrix},$$

and the sparsity pattern matrix is defined as

$$\mathbf{E} = \begin{bmatrix} \mathbf{1}_{6\times3} & \mathbf{0}_{6\times7} & \mathbf{0}_{6\times7} \\ \mathbf{0}_{6\times3} & \mathbf{1}_{6\times7} & \mathbf{0}_{6\times7} \\ \mathbf{0}_{6\times3} & \mathbf{0}_{6\times7} & \mathbf{1}_{6\times7} \end{bmatrix},$$

where $\mathbf{1}_{p\times q} \in \mathbb{R}^{p\times q}$ is a p by q matrix filled with ones. The sparsity matrix defines that AUV 1 has access to the first 3 entries of the total measurement vector, agent 2 to the following 7 entries, and agent 3 has access to the remaining ones. Note that, upon setting a measurement ordering for the centralized observation matrix, that same ordering must be kept when building the measurement vector of each agent.

Consider the vector $\mathbf{y}_{ij}(t_k) := \left[\mathbf{0}_{1\times3} \quad z_i(t_k) - z_j(t_k)\right]^T$, where z_i and z_j are the depth measurements obtained by AUVs with indices i and j, respectively. Let $\boldsymbol{\Delta}_{ij}(t_k) = \mathbf{p}_i(t_k) - \mathbf{p}_j(t_k)$ and

$$\mathbf{P}_{ij}(t_k) = \begin{bmatrix} & \bar{\mathbf{D}}_{ij}(t_k) & \\ 0 & 0 & 1 \end{bmatrix},$$

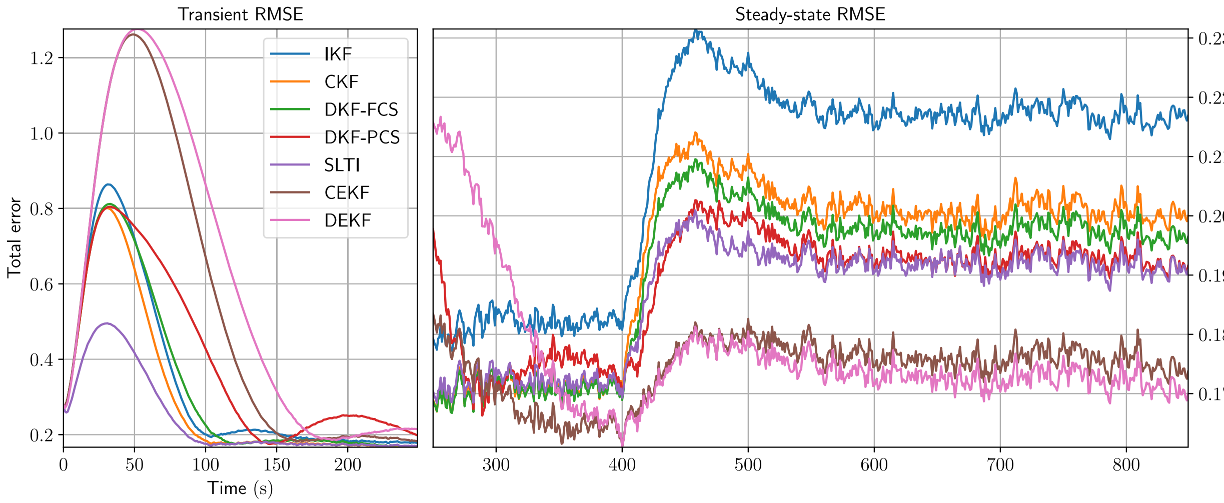

(a) Acyclical topology RMSE results of observers tuned for steady-state performance.

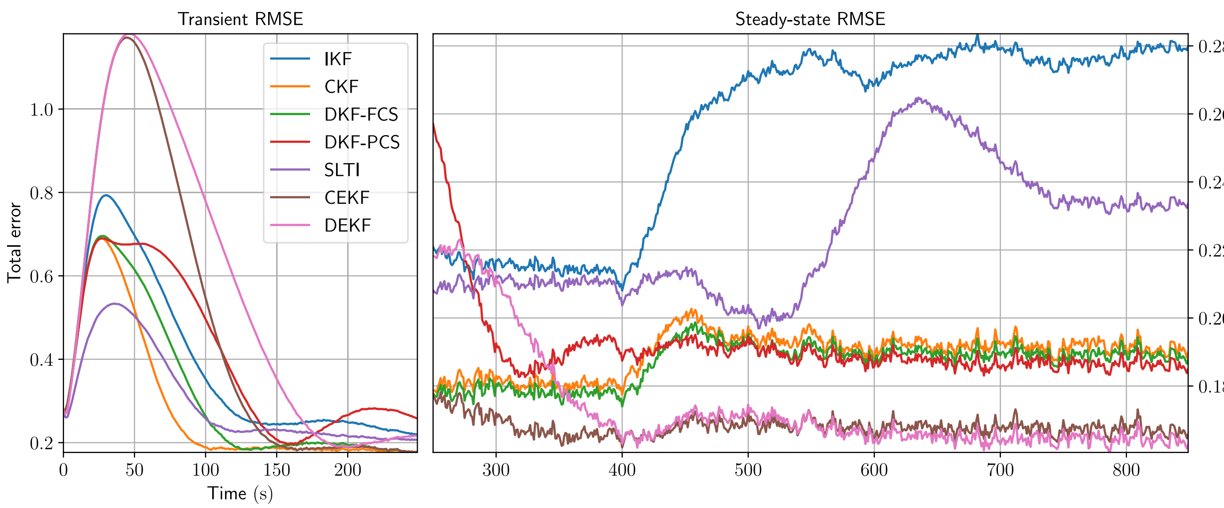

(b) Cyclical topology RMSE results of observers tuned for steady-state performance.

Fig. 6. RMSE results of algorithms tuned for steady-state performance.

with $\bar{\mathbf{D}}_{ij}$ defined as in (16). One then has that

$$\mathbf{P}_{ij}(t_k)\boldsymbol{\Delta}_{ij}(t_k) = \mathbf{y}_{ij}(t_k),$$

from which it is possible to recover $\boldsymbol{\Delta}_{ij}(t_k)$ as

$$\boldsymbol{\Delta}_{ij}(t_k) = \left(\mathbf{P}_{ij}^T(t_k)\mathbf{P}_{ij}(t_k)\right)^{-1}\mathbf{P}_{ij}^T(t_k)\mathbf{y}_{ij}(t_k),$$

provided that $\mathbf{P}_{ij}^T(t_k)\mathbf{P}_{ij}(t_k)$ is invertible, which is the case if $z_i(t_k) - z_j(t_k) \neq 0$.

Rather than actual relative position measurements, the vector entries, $\mathbf{m}_{ij} \in \mathbb{R}^3$, of $\mathbf{m}_i$, are instead taken as

$$\mathbf{m}_{ij}[k+1] = \alpha_{ij}\boldsymbol{\Delta}_{ij}(t_{k+1}) + (1-\alpha_{ij})\mathbf{D}_{ij}(t_{k+1})(\hat{\mathbf{p}}_i(t_{k+1}|t_k) - \hat{\mathbf{p}}_j(t_{k+1}|t_k)),$$

with $\mathbf{D}_{ij}$ defined in (15). Each artificial relative position measurement is given by a weighted sum of the extracted position difference, $\boldsymbol{\Delta}_{ij}$, and the projection of its current prediction, $\mathbf{D}_{ij}(\hat{\mathbf{p}}_i - \hat{\mathbf{p}}_j)$, with $\hat{\mathbf{p}}_i$ and $\hat{\mathbf{p}}_j$ extracted from $\hat{\mathbf{x}}_i[k+1|k]$ and $\hat{\mathbf{x}}_j[k+1|k]$, respectively. This projection is done using $\mathbf{D}_{ij}(t_{k+1})$, which is constructed using the measured bearing angles via $\mathbf{d}_{ij}(t_{k+1})$, according to (6) and (15). Since the matrix $\mathbf{P}_{ij}^T\mathbf{P}_{ij}$ becomes close to singular if the height difference between the agents is close to zero, causing numerical instability, the weights are chosen as $\alpha_{ij} = |\mathbf{d}_{ij}^z(t_{k+1})|$. This ensures that when the extracted position difference, $\boldsymbol{\Delta}_{ij}$, is unreliable, the bearing measurement information can still be used.

5. Simulation results

5.1. Setup

The setup considered for simulation analysis consists of a set of 10 AUVs performing a mission, whereby the agents must visit a set of waypoints while maintaining a certain formation. The agents start with the spatial distribution presented in Fig. 2(a), and maintain this formation for a portion of their mission. Then, they change to a different spatial distribution, as represented in Fig. 2(b). They accomplish this by stopping until all have reached their waypoints, and then moving towards their next location in the formation until they reach it. Once all agents are in their respective locations, they move on to the next waypoint. Fig. 3 shows the nominal trajectory of agent 1.

The fluid velocity, $\mathbf{v}_{f_i} = \begin{bmatrix}0.1 & -0.2 & 0\end{bmatrix}^T$ (m s^{-1}), was assumed to be constant throughout the whole operating space for all $i \in \mathcal{V}$, where $\mathcal{V}$ is the set of AUVs. The relative velocity of each agent, $\mathbf{v}_{r_i}(t)$, is available at a rate of 50 Hz and is corrupted by additive zero mean white Gaussian noise, with covariance matrix $\boldsymbol{\Sigma}_u = 0.01^2\mathbf{I}_3$. The agents have access to their orientation, parameterized by its roll, pitch, and yaw Euler angles. These are also corrupted by independent additive zero-mean white Gaussian noise, with standard deviation of 0.05° for the roll and pitch angles, and 0.3° for the yaw angle. The control signal

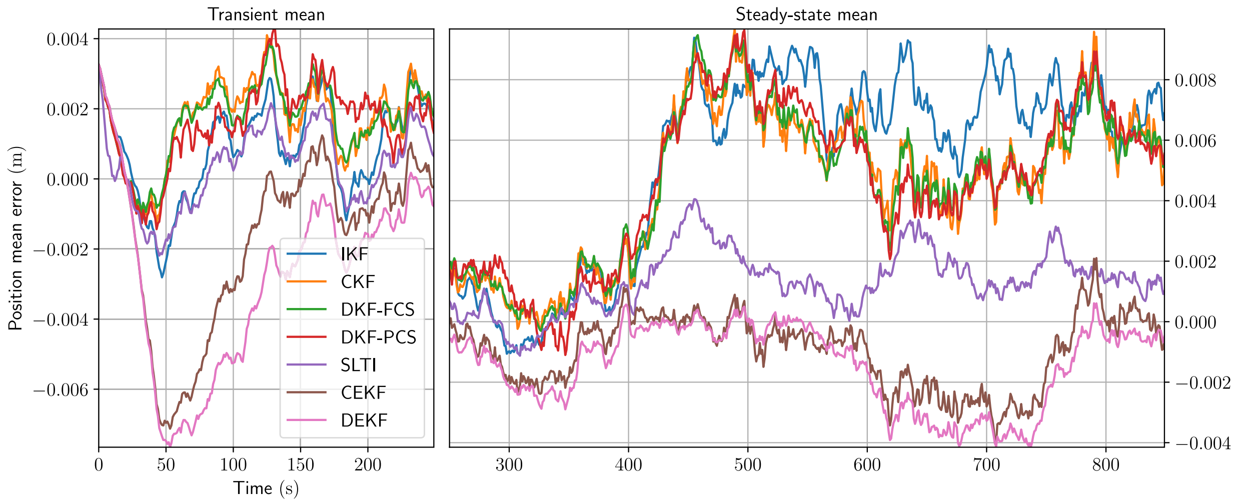

(a) Acyclical topology mean $\mathbf{p}_3^x$ estimation error of observers tuned for steady-state performance.

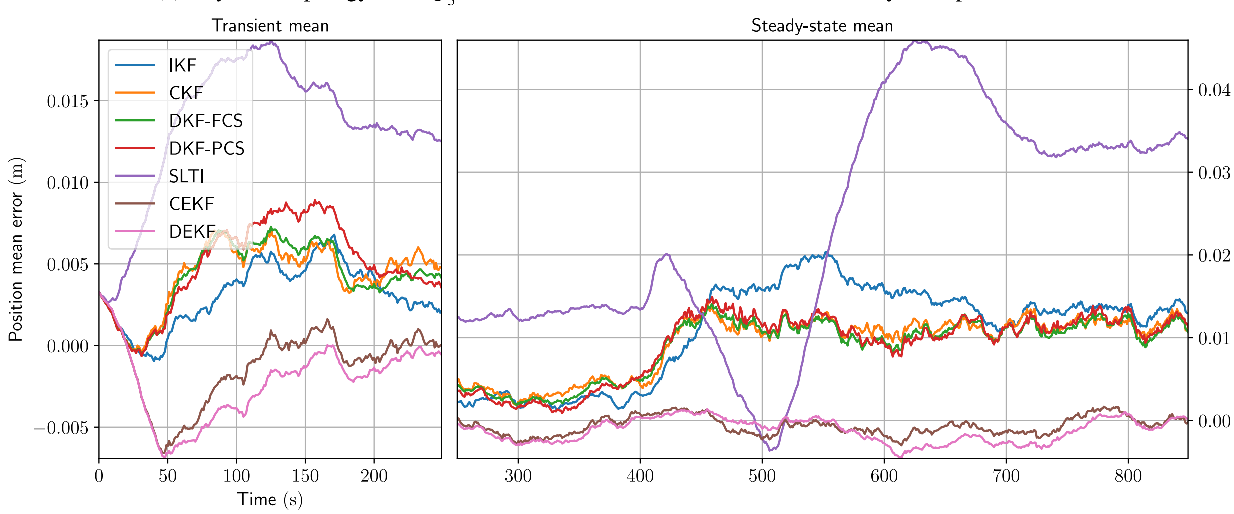

(b) Cyclical topology mean $\mathbf{p}_3^x$ estimation error of observers tuned for steady-state performance.

Fig. 7. Mean $\mathbf{p}_3^x$ estimation error of observers tuned for steady-state performance.

of each agent, $\mathbf{u}_i[k]$, is obtained using the trapezoidal integration rule of $\mathbf{R}_i(t)\mathbf{v}_{r_i}(t)$ between measurement time steps, approximating (2).

The AUVs capture measurements every $T = 1\,\mathrm{s}$. Leaders obtain measurements of their position corrupted by additive zero mean white Gaussian noise, with covariance matrix $\boldsymbol{\Sigma}_{\mathrm{pos}} = 0.1^2\mathbf{I}_3$, and the depth measurements of the follower AUVs are corrupted by additive zero mean white Gaussian noise, with standard deviation of $0.1\,\mathrm{m}$. The measured bearing angles, θ and ϕ, captured in the measuring agent's body frame, are corrupted by additive independent zero mean Gaussian noise, with standard deviation of 1°.

The process noise covariance matrix of each AUV is given by $\mathbf{Q}_i = \mathrm{diag}\left(0.05^2\mathbf{I}_3, 0.005^2\mathbf{I}_3\right)$. The measurement noise covariance matrix for absolute position measurements is given by $\mathbf{R}_{\mathrm{pos}} = 0.1^2\mathbf{I}_3$, and the noise corrupting depth measurements is modeled with a standard deviation of $\sigma_d = 0.1\,\mathrm{m}$. All agents are assumed to be completely uncorrelated at time $t = 0$, such that all the cross-covariance matrices and factors between agents are equal to the zero matrix, $\mathbf{0}_6$. In order to compute the steady-state gains for the static gain observer, (18) and (19) were propagated until $|\,\mathrm{tr}\,(\boldsymbol{\Sigma}[k+1|k+1]) - \mathrm{tr}\,(\boldsymbol{\Sigma}[k|k])\,| < 0.001$, where $\mathrm{tr}(\cdot)$ is the trace operator. The observers will be studied using two separate sets of tuning parameters, one tuned for convergence, and the other for steady-state behavior. The remaining filter parameters will be specified in each case.

The considered measurement topologies are presented in Figs. 4(a) and 4(b). The agents are organized by tiers, such that $\mathcal{T}_0 = \{1,2\} = \mathcal{V}_L$, $\mathcal{T}_1 = \{3,4,5,6\}$, and $\mathcal{T}_2 = \{7,8,9,10\}$ are the sets of agents in tiers 0, 1, and 2, respectively. Note that there are two leaders, agents 1 and 2, and they both are at the top of the formation, in tier 0. The cycles were made by flipping some of the edges (highlighted in green in Fig. 4(b)) between tiers 1 and 2 in the acyclical topology, and by introducing the blue edges around each tier of agents.

In order to evaluate the transient response and the steady-state performance of the presented estimators, the algorithms were implemented on each agent and $N = 500$ runs of the mission were simulated. The root-mean-squared-error (RMSE) of the position and fluid velocity estimates, obtained for each time instant from the collection of Monte Carlo runs, was then computed, such that

$$\mathrm{RMSE}(\mathbf{x}[k]) = \sqrt{\frac{\sum_{n=1}^{N} \|\mathbf{x}[k] - \hat{\mathbf{x}}^n[k]\|^2}{N}},$$

where $\mathbf{x}[k]$ is the concatenation of the state vectors of all AUVs at time k, and $\hat{\mathbf{x}}^n[k]$ is its estimate obtained in the nth Monte Carlo run.

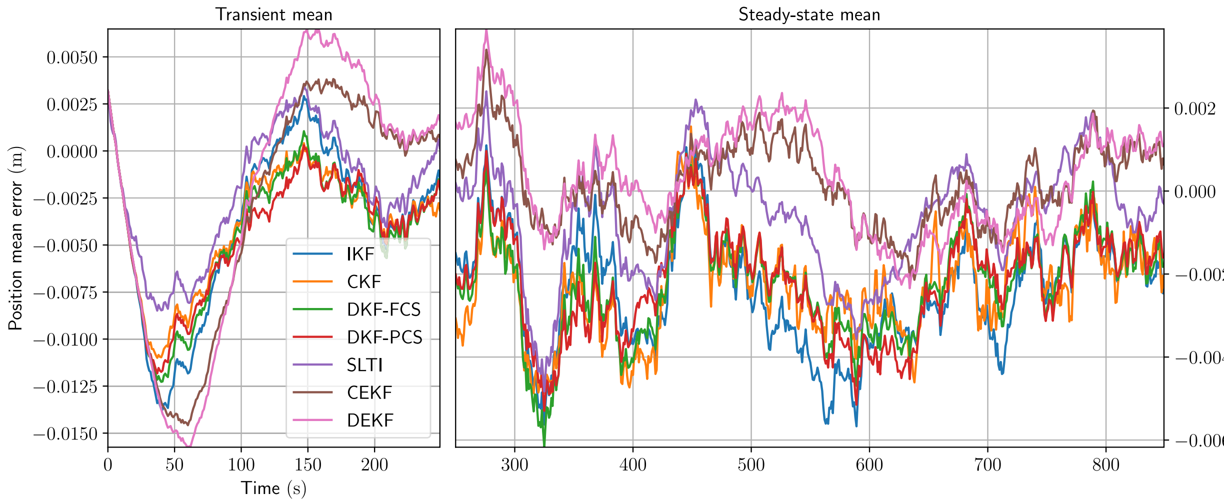

(a) Acyclical topology mean $\mathbf{p}_9^x$ estimation error of observers tuned for steady-state performance.

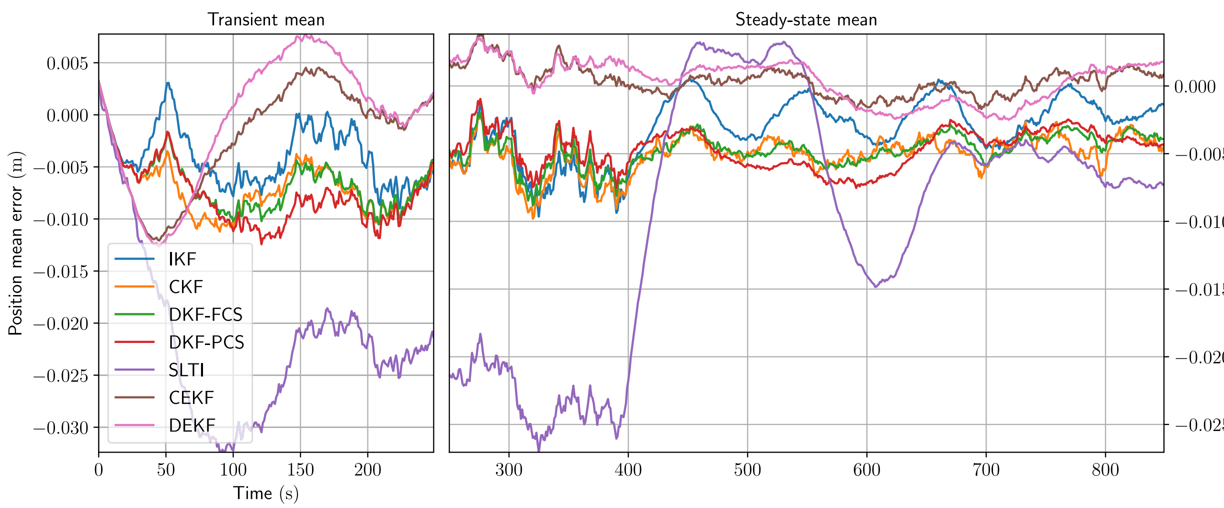

(b) Cyclical topology mean $\mathbf{p}_9^x$ estimation error of observers tuned for steady-state performance.

Fig. 8. Mean $\mathbf{p}_9^x$ estimation error of observers tuned for steady-state performance.

Additionally, in order to investigate whether the estimators are biased, the mean error of the estimated quantities, for each time instant, was computed from the collection of Monte Carlo runs, as given by

$$\text{mean}(\mathbf{x}[k]) = \frac{1}{N}\sum_{n=1}^{N} \mathbf{x}[k] - \hat{\mathbf{x}}^n[k].$$

5.2. Results

Due to the specific tuning parameters used in order to achieve good steady-state performance, the algorithms can take a while to converge. In order to improve the convergence time of these solutions, separate tuning parameters can be used, depending on the phase of the mission. Initially, if the agents are completely unlocalized, they can adopt a certain set of tuning parameters optimized for convergence speed. After a certain amount of time, they can change to parameters optimized for steady-state performance. These parameters were set empirically, as is the case with most nonlinear estimation problems. Taking this into account, the convergence of the algorithms was studied separately from their steady-state performance. Firstly, the convergence behavior of the presented solutions is studied. Then, the steady-state behavior is analyzed by considering small initial estimation errors.

5.2.1. Convergence analysis

For the EKF-based approaches, the initial state estimate for each of the Monte Carlo runs was sampled from a Gaussian distribution with mean identical to the true value and with covariance matrix $\boldsymbol{\Sigma}_0 = \text{diag}(10^2\mathbf{I}_3, \mathbf{I}_3)$, whereas for the remaining ones the initial state estimates were sampled from a Gaussian distribution with covariance matrix $\boldsymbol{\Sigma}_0 = \text{diag}(250^2\mathbf{I}_3, 50^2\mathbf{I}_3)$ and mean identical to the true value. The initial state covariance matrix of each agent was likewise set as $\boldsymbol{\Sigma}_{ii}[0|0] = \text{diag}(50^2\mathbf{I}_3, 10^2\mathbf{I}_3)$ and the noise affecting the relative measurement between AUVs is modeled with the covariance matrix $\mathbf{R}_b = 0.01^2\mathbf{I}_2$ for EKF-based approaches, and $\mathbf{R}_b = 0.5^2\mathbf{I}_3$ for the remaining ones. The initial 400 seconds of the full mission were simulated $N = 500$ times, with the specified simulation and tuning parameters, considering independent noise vectors for each run.

It is well known that EKF-based approaches do not guarantee global convergence and require relatively accurate initial state estimates. How accurate these initial estimates must be depends on both the spatial distribution of the agents in the formation, as well as their measurement topology. The number of convergent runs, under each topology, for both the CEKF and DEKF, are presented in Table 1. Similar results were obtained for different formation configurations, and show that the

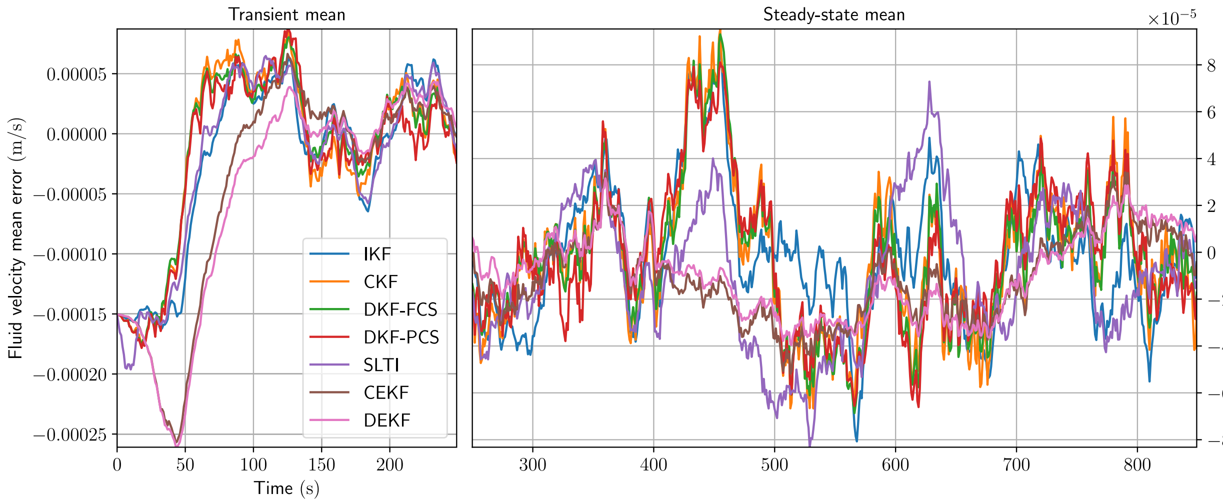

(a) Acyclical topology mean $\mathbf{v}_{f_3}^x$ estimation error of observers tuned for steady-state performance.

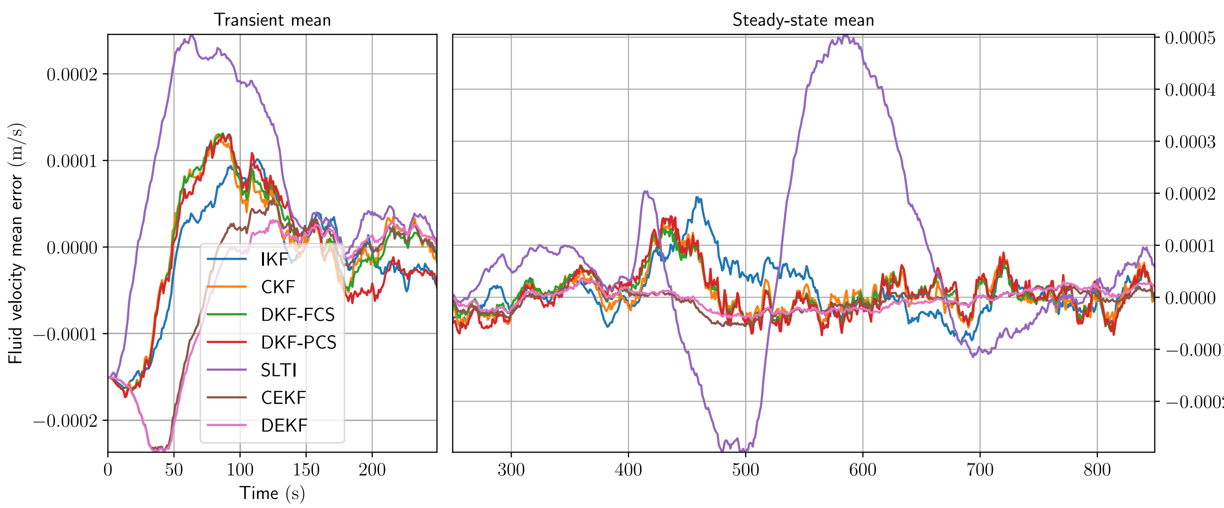

(b) Cyclical topology mean $\mathbf{v}_{f_3}^x$ estimation error of observers tuned for steady-state performance.

Fig. 9. Mean $\mathbf{v}_{f_3}^x$ estimation error of observers tuned for steady-state performance.

Table 1
Number of convergent runs (and respective convergence percentage) for each EKF-based estimator under the acyclical and cyclical measurement topologies.

	Acyclical	Cyclical
CEKF	443 (88.6 %)	448 (89.6 %)
DEKF	463 (92.6 %)	487 (97.4 %)

centralized approach is more sensitive to the initial conditions of the agent configuration than its decentralized counterpart, emphasizing the inherent robustness of decentralized approaches. Since the CEKF shares more information, its estimates are also more affected by erroneous initial state estimates, hence the added difficulty in converging. As for the linear estimators, their estimates converged to the true solution on all runs. The RMSE of the convergent estimates obtained by each of the considered estimators, for both measurement topologies, is presented in Figs. 5(a) and 5(b).

In these figures, besides the CEKF and DEKF, the other approaches are labeled as follows. The approach presented in Section 4.1 is labeled as IKF; the centralized Kalman filter approach, presented in 4.2, is labeled as CKF; and the two variants of its decentralized counterpart, presented in Section 4.3, are labeled as DKF-FCS and DKF-PCS. DKF-FCS reproduces the whole joint covariance matrix (17), whereas DKF-PCS keeps communication to a minimum and does not fill the entries corresponding to cross-covariances between neighbors of the measuring agent. Lastly, the static-gain observer presented in Section 4.4 is labeled as SLTI.

As shown in Fig. 5(a), all the linear observers, except SLTI, produced estimates that converged to the true solution in just a few time-steps when the measurement topology is acyclical. SLTI does not achieve this because it is a static-gain observer designed for steady-state performance, which typically involves low gains, thus the slow convergence.

Upon introduction of new edges to form cycles, the convergence speed of the IKF is severely affected, as shown in Fig. 5(b). This is related to the fact that each agent following this observer design produces its estimates independently of the other AUVs, disregarding possible cross-measurement information. The other linear time-varying Kalman filter approaches, however, converge to the solution unaffected by the presence of cycles in the measurement graph. Similarly, the convergence speed of the SLTI is only slightly affected by the introduction of these edges.

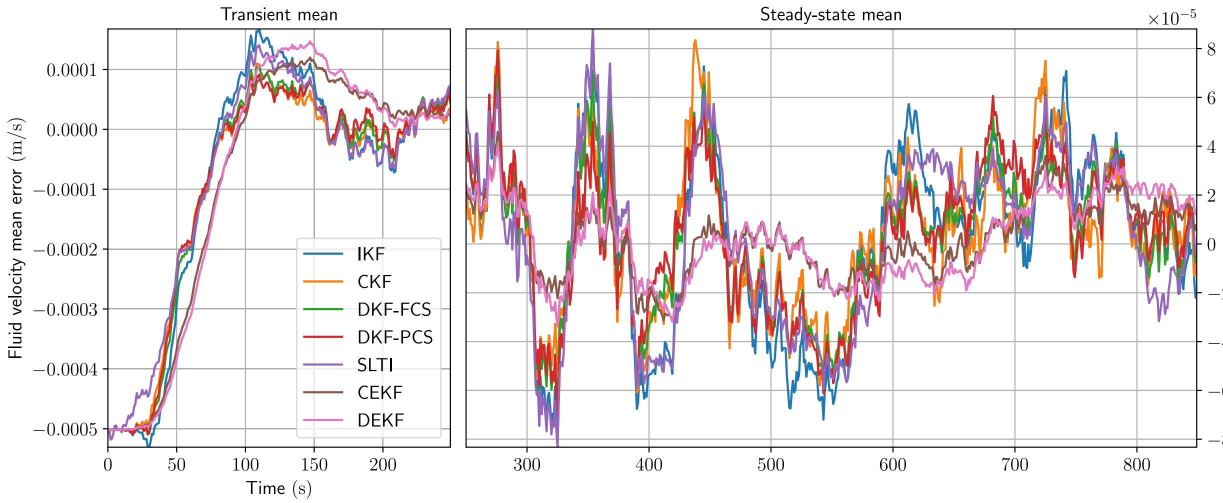

(a) Acyclical topology mean $\mathbf{v}_{f_9}^{x}$ estimation error of observers tuned for steady-state performance.

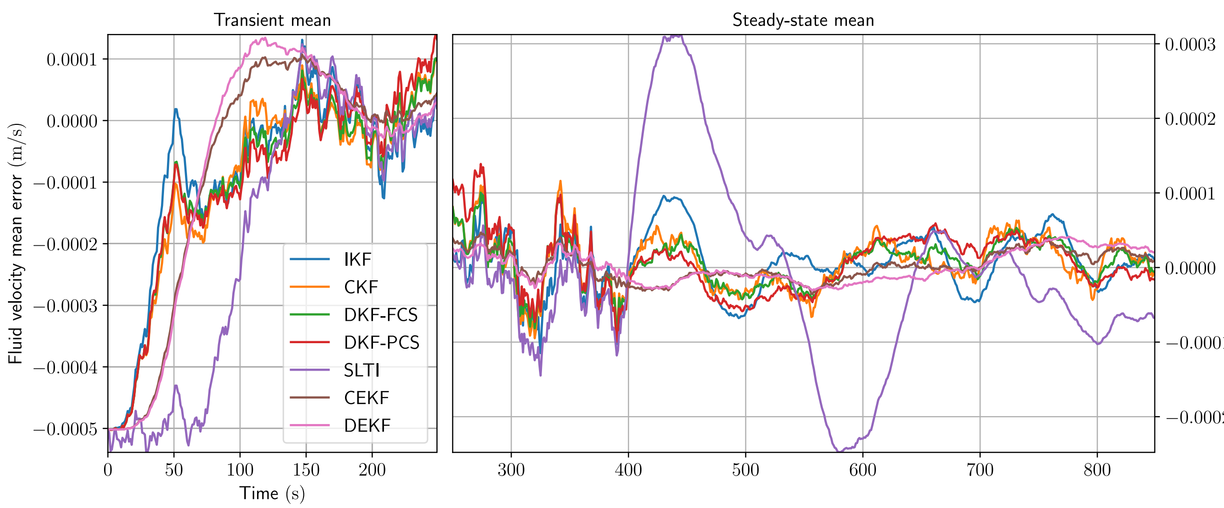

(b) Cyclical topology mean $\mathbf{v}_{f_9}^{x}$ estimation error of observers tuned for steady-state performance.

Fig. 10. Mean $\mathbf{v}_{f_9}^{x}$ estimation error of observers tuned for steady-state performance.

5.2.2. Steady-state performance

Here, the RMSE of the estimates obtained with each estimator, tuned for steady-state performance, is compared. Since the observers were optimized for steady-state performance, their convergence is quite slow. Thus, the initial state estimates were set very close to their real value by sampling them from a Gaussian distribution, centered at the real state vectors and with covariance matrix $\boldsymbol{\Sigma}_0 = \mathrm{diag}(0.05^2\mathbf{I}_3, 0.01^2\mathbf{I}_3)$. The initial covariance matrix of each agent was set as $\boldsymbol{\Sigma}_{ii}[0|0] = \boldsymbol{\Sigma}_0$ and the artificial measurements' covariance matrix was set as $\mathbf{R}_b = 0.3^2\mathbf{I}_2$ for the EKF-based estimators, and $\mathbf{R}_b = 3^2\mathbf{I}_3$ for the remaining ones. The RMSE results for the acyclical topology are presented in Fig. 6(a), and for the cyclical measurement topology in Fig. 6(b).

The IKF has the worst performance of the considered estimators. As mentioned before, this is because the IKF keeps no cross-measurement information, whereas all the other estimators do some way or the other. Also, contrary to what one would expect, the CKF does not have the best performance out of the estimators in its class, which is due to the presence of a non-zero error bias in the artificial quantities built from the bearing angles. Indeed, the expected value of the direction vector, built according to (6), considering noisy measurements, is not equal to the nominal direction vector built from noiseless bearing angles. Since the centralized approaches make use of more information to produce their estimates and, in this case, fail to account for biased errors, this additional information ends up being detrimental to the filter's performance, depending on the tuning parameters. The CEKF and the DEKF have the best performance, which is because they use the bearing angles directly (after rotation to the inertial frame), unlike the other algorithms, and thus are not affected by the measurement error bias originating from the construction of the direction vector. Note, however, that rotating the bearing angles to the inertial frame can still result in the introduction of a bias into the estimation error due to the noisy attitude measurements, resulting in the DEKF presenting better estimation capabilities than the CEKF.

The introduction of cycles was detrimental to the performance of the IKF, which, again, is due the fact that it keeps no cross-measurement information, and thus the estimation errors are re-fed to the estimation algorithm with no regard for where they originated from, resulting in difficulties in converging and higher RMSE. SLTI has also seen its performance severely decreased. However, this is due to the fact that the blue edges concern agents which are at the same height, and, as mentioned before, the matrices $\mathbf{P}_{ij}$ become singular when this happens, resulting in numerical instability. The CEKF and DEKF have benefited from the introduction of cycles, since their RMSE is lower. Likewise, the other estimators, CKF, DKF-FCS, and DKF-PCS, saw their performance slightly improved. The introduction of new edges and cycles has allowed the algorithms to work with more information and create better correlation between the agents. However, the biasing errors for CKF, DKF-FCS, and DKF-PCS, make it so fine-tuning is still required in order to balance measurement information with the amount of biasing error, which depends on both the measurement topology and spatial formation.

In the following, the presence of a non-zero estimation error bias is investigated. For that effect, the mean results for the x coordinate of the estimated positions and fluid velocities of AUVs 3 and 9 are presented in Figs. 7 to 10. Regardless of the measurement topology, there is a clear non-zero estimation error bias for the linear estimators, though it is very small given these parameters, and the estimators still provide a good enough estimate for most purposes. This bias is dependent on the spatial formation of the agent, and comes mostly from the construction of the artificial direction vectors, $\mathbf{d}_{ij}$. Since the EKF-based approaches use the bearing angles directly (after rotation to the inertial frame), the noise affecting the measurement vector of these approaches is closer to a normally distributed noise than the one affecting the other approaches, hence there is no noticeable bias in these approaches' results. As for the fluid velocity, there is no clear estimation error bias, though there is no guarantee that there will not be one, since the control input, $\mathbf{u}[k]$, is computed using the noisy rotation matrix.

5.2.3. Further comments

While no results were presented for sampling times other than $T = 1\,\mathrm{s}$, or for sensor failure events, some comments can be made regarding their effects on the generated navigation estimates. A smaller sampling time will allow the system to receive more information, which will reduce its convergence time, and, in the case of the EKF-based approaches, will make them less sensitive to the initial estimation error. However, the attitude measurements captured by the AUVs are corrupted by attitude noise, and these are then used to create the prediction estimate. Given the same tuning parameters, due to the system having a lower sampling time and thus receiving more information, which might be affected by a biased error, this extra information might end up pushing the system's estimates away from the true value. Regardless, by adjusting the tuning parameters to the sampling time, it is possible to produce better estimates than with a higher sampling time.

Regarding sensor failures, these can be events where no data is captured by an agent, as well as events where outlier data is exchanged. There exist several alternatives for dealing with this problem, such as the one presented in Navon and Bobrovsky (2021), though these are out of the scope of this paper. Regardless, solutions based on artificial measurements have a major advantage when compared to the EKF-based ones when it comes to total sensor failure, that is, events where the AUV receives no measurement information. Since the former type of solutions can be guaranteed to converge for acyclical formations, the frequency of sensor failure can be arbitrarily high and the generated estimate will still eventually converge to a neighborhood of the true state of the system. However, EKF-based solutions are not guaranteed to converge, and thus can be very sensitive to sensor failures, especially if those cause outlier data to be exchanged between agents without being filtered out. Given a high enough frequency of these events, EKF-based solutions might even diverge.

As a final note on computational complexity: centralized approaches scale, in general with the square of the total number of agents. As an example, a centralized approach implemented for a team of 20 agents will require a central location, or in some implementations, every single AUV, to carry and perform inversion operations involving a covariance matrix $\boldsymbol{\Sigma}[k] \in \mathbb{R}^{120\times120}$, which has a total of 14400 entries. By comparison, in decentralized approaches, the computational complexity scales differently for each agent and is dependent on the measurement topology, scaling instead with the square of number of neighbors at each agent. This, in general, does not scale with the total number of agents and is usually a small number. Additionally, the larger the number of AUVs, the more robust the communication links have to be, since any link failure will lead to missing inputs in the prediction and update steps.

6. Conclusion

In this study, both centralized and decentralized cooperative navigation techniques were described and evaluated. Centralized approaches require all data to be manipulated at a single location, which makes these approaches unfeasible in practice. Due to the distance between agents and the fact that communication underwater is very limited, not only in range, but also in latency, it is very hard, if not impossible, to gather all measurements at a single location with full synchronicity. Decentralized solutions do not suffer from this problem, making them superior to centralized approaches when the communication links are fragile. Taking into account the additional computational complexity and communication requirements discussed in the previous section, it is then possible to conclude that, in most cases, the potential gain in performance obtained from using a centralized approach does not outweigh the additional difficulties in implementing it when compared with a decentralized approach.

The EKF-based approaches were compared with artificial measurement based ones, under both acyclical and cyclical measurement topologies. While the latter approaches, which are based on linear measurements, present better convergence qualities when compared to EKF-based ones, this comes at the cost of changing the noise characteristics of the measurement error vector, which prevents Kalman filter implementations from providing unbiased estimates, worsening their performance. As such, a combination of both these types of approaches should be considered, whereby an artificial measurement based filter can be used at the start of the mission, switching to and EKF-based approach when sufficiently good navigation performance has been achieved. In both the convergence and steady-state analysis of the algorithms, the decentralized approaches outperformed the centralized ones.

CRediT authorship contribution statement

Pedro Mendes: Analysis, Investigation, Software, Data gathering, Writing – original draft, Writing – review & editing. **Pedro Batista:** Conceptualization, Funding acquisition, Methodology, Supervision, Writing – original draft, Writing – review & editing. **Paulo Oliveira:** Conceptualization, Methodology. **Carlos Silvestre:** Conceptualization, methodology.

Declaration of competing interest

The authors declare that they have no known competing financial interests or personal relationships that could have appeared to influence the work reported in this paper.

Data availability

Data will be made available on request.

Acknowledgments

Funding

This work was supported by the Fundação para a Ciência e a Tecnologia (FCT) through LARSyS — FCT project [grant number UIDB/50009/2020]; by the FCT, Programa Operacional Regional de Lisboa 2020 and PIDDAC programs through the FCT project DECENTER [grant number LISBOA-01-0145-FEDER-029605]; by the European Union's Horizon 2020 research and innovation programme [grant number 101017808]; by the Macau Science and Technology Development Fund [grant number FDCT/0146/2019/A3]; and by the University of Macau [grant number MYRG2020-00188-FST].

References

Bahr, A., Walter, M.R., Leonard, J.J., 2009. Consistent cooperative localization. In: 2009 IEEE International Conference on Robotics and Automation. IEEE, pp. 3415–3422.

Carrillo-Arce, L.C., Nerurkar, E.D., Gordillo, J.L., Roumeliotis, S.I., 2013. Decentralized multi-robot cooperative localization using covariance intersection. In: 2013 IEEE/RSJ International Conference on Intelligent Robots and Systems. IEEE, pp. 1412–1417.

Fallon, M.F., Papadopoulos, G., Leonard, J.J., 2010. A measurement distribution framework for cooperative navigation using multiple AUVs. In: 2010 IEEE International Conference on Robotics and Automation. IEEE, pp. 4256–4263.

Gelb, A., 1974. Applied optimal filtering. The MIT Press.

Jazwinski, A., 1970. Stochastic Processes and Filtering Theory. Academic Press, Inc.

Kia, S.S., Rounds, S., Martinez, S., 2016. Cooperative localization for mobile agents: A recursive decentralized algorithm based on Kalman-filter decoupling. IEEE Control Syst. Mag. 36, 86–101.

Luft, L., Schubert, T., Roumeliotis, S.I., Burgard, W., 2018. Recursive decentralized localization for multi-robot systems with asynchronous pairwise communication. Int. J. Robot. Res. 37, 1152–1167.

Mendes, P., Batista, P., 2021. A study on cooperative navigation of AUVs based on bearing measurements. In: OCEANS 2021: San Diego – Porto. pp. 1–8. http://dx.doi.org/10.23919/OCEANS44145.2021.9705838.

Navon, E., Bobrovsky, B.-Z., 2021. An efficient outlier rejection technique for Kalman filters. Signal Process. 188, 108164.

Reis, J., Morgado, M., Batista, P., Oliveira, P., Silvestre, C., 2016. Design and experimental validation of a usbl underwater acoustic positioning system. Sensors 16, 1491.

Safavi, S., Khan, U.A., Kar, S., Moura, J.M., 2018. Distributed localization: A linear theory. Proc. IEEE 106, 1204–1223.

Santos, D., Batista, P., Oliveira, P., Silvestre, C., 2021. Decentralised navigation systems for bearing-based position and velocity estimation in tiered formations. Int. J. Syst. Sci. 1–22.

Viegas, D., Batista, P., Oliveira, P., Silvestre, C., 2016. Decentralized state observers for range-based position and velocity estimation in acyclic formations with fixed topologies. Int. J. Robust Nonlinear Control 26, 963–994.

Viegas, D., Batista, P., Oliveira, P., Silvestre, C., 2018. Discrete-time distributed Kalman filter design for formations of autonomous vehicles. Control Eng. Pract. 75, 55–68.